A Method to Include the Available Information of Disturbances in the Modifier Adaptation Methodology for Real-Time Optimization

Daniel Navia[a], Antonio Puen[a], Paulina Quintanilla[a], Luis Briceño[b], Luis Bergh[a]

[a]*Departamento de Ingeniería Química y Ambiental, Universidad Técnica Federico Santa María*
[b]*Departamento de Matemática, Universidad Técnica Federico Santa María*

Abstract

In this work, we propose the inclusion of the available information of measured or estimated disturbances in the modifier adaptation methodology for real-time optimization (RTO). The idea is to extend the applicability of this technique for processes wherein disturbances affect the quantities involved in the necessary optimality conditions of the process. To do so, we include the estimation of process gradients with respect to both decision variables and disturbances in the methodology. The implementation of this approach was performed in a laboratory-scale flotation column, where the effects of changes in the feed characteristics on the economic performance were included. Additionally, the impact of the availability of disturbances information was analyzed, considering immediate and delayed availability. In the latter case, the Auto Regressive Integrated Moving Average model (ARIMA) was used as an estimator in each RTO iteration. The results show that the inclusion of the available information of disturbances allows tracking the optimum of the process under continuously changing feed conditions.

Keywords: Real Time Optimization, Modifier adaptation, Disturbances, Flotation Column, Process Optimization.

Highlights

Changes in disturbances can compromise the KKT matching in modifier adaptation method

Including the disturbances in gradient estimation allows tracking the NOC of a process

Implementation of modifier adaptation in laboratory using real data of disturbances

Columnar flotation can increase its economic performance in 26%

A Method to Include the Available Information of Disturbances in the Modifier Adaptation Methodology for Real-Time Optimization

Daniel Navia[a], Antonio Puen[a], Paulina Quintanilla[a], Luis Briceño[b], Luis Bergh[a]

[a]*Departamento de Ingeniería Química y Ambiental, Universidad Técnica Federico Santa María*
[b]*Departamento de Matemática, Universidad Técnica Federico Santa María*

Abstract

In this work, we propose the inclusion of the available information of measured or estimated disturbances in the modifier adaptation methodology for real-time optimization (RTO). The idea is to extend the applicability of this technique for processes wherein disturbances affect the quantities involved in the necessary optimality conditions of the process. To do so, we include the estimation of process gradients with respect to both decision variables and disturbances in the methodology. The implementation of this approach was performed in a laboratory-scale flotation column, where the effects of changes in the feed characteristics on the economic performance were included. Additionally, the impact of the availability of disturbances information was analyzed, considering immediate and delayed availability. In the latter case, the Auto Regressive Integrated Moving Average model (ARIMA) was used as an estimator in each RTO iteration. The results show that the inclusion of the available information of disturbances allows tracking the optimum of the process under continuously changing feed conditions.

Keywords: Real Time Optimization, Modifier adaptation, Disturbances, Flotation Column, Process Optimization.

1. Introduction

In the process industry, a large number of variables can be manipulated to improve production and achieve financial aims. Consequently, finding an optimal point is not a trivial task, due to the uncertainties and disturbances that continuously modify the operating conditions. To remain competitive, the enterprises must face a growing need for being more economically efficient, safer and more sustainable. With regard to process supervision, attaining improvements in efficiency requires achieving optimal operational points.

However, there is an inherent difficulty in getting plants to reach optimal operating points, since models only partially represent the process phenomenology. Furthermore, a large number of variables associated with other stages of the process could modify the economic performance. From the mathematical point of view, this makes the task of finding optimal points more complex, because there is modeling mismatch to consider along with the disturbances that constantly modify the conditions of the operation.

Real-time optimization (RTO) can be a tool to achieve industry goals. In the plant decision hierarchy, RTO is located as a layer of operation at a higher level than control systems and lower than layers such as planning and scheduling. Upper layers give instructions to lower layers, and the

former send information as feedback to the latter. Therefore, applying RTO makes it possible to have economic decisions be implemented in the plant in real time.

RTO emerged in the 1970s as a two-stage algorithm that contemplated parametric estimation and economic optimization. This methodology, proposed by Bamberger & Isermann (1978), consists of an initial stage of parametric estimation of a nonlinear model and then the optimization of a performance index with the updated model. Although this method can arbitrarily handle complex systems with many degrees of freedom, it was demonstrated that the parametric estimation is not adequate under a scenario of structural uncertainty.

Therefore, on account of the fact that the two-stage approach has difficulty converging to the optimum of the process, a modified two-stage approach was developed by Roberts (1979), and it was called Integrated System Optimization and Parameter Estimation (ISOPE). This methodology requires calculating plant gradients of output variables from the process (i.e.,$\boldsymbol{y}$) with respect to the inputs ($\boldsymbol{u}$), in order to introduce a term that modifies the objective function of the economic optimization, adding a first order corrector. Subsequently, the parameter estimation step was eliminated, and correction terms were added to the optimization problem. These terms take into account the differences between the real process and model output derivatives with respect to decision variables (Tatjewski, 2002).

More than two decades later, adding a correction term in the inequality constraints of the optimization problem was proposed by Gao & Engell (2005), due to supposition that the constraints are affected by model uncertainty. Later, the Modifier Adaptation methodology (MA) was defined, first by Chachuat et al. (2009) and afterward by Marchetti et al. (2009). The main characteristic of this methodology is KKT matching between the plant and model problem and the modified optimization problem, which can find the optimal operation of an uncertain process (Marchetti et al., 2016).

In the last few years, the research has made considerable advancements by using the methodology (MA) as a basis for the following studies. The more recent investigations have been focused on improving this technique, whether by searching for a more reliable and robust gradient estimation (Bunin et al., 2012; Marchetti et al., 2010) or by avoiding the gradient estimation step (Gao et al., 2016; Navia et al., 2015).

Regarding MA applications, it has been performed with few input variables and with known noise characteristics. That occurs for two reasons: (i) fewer points are required for gradient estimation, and (ii) there is less difficulty in handling since these are less sophisticated systems. Additionally, in MA applications, it is assumed that the sampling time of the disturbances is longer than the settling time (Darby et al., 2011).

The first aspect, mentioned above, has been addressed by Costello et al. (2016) with their Directional Modifier Adaptation method (D-MA) that can handle a large number of input variables ($\boldsymbol{n_u}$). The disturbances issue is approached in this work, assuming that the disturbances are input variables coming from another stage, with a sampling time shorter than the settling time of the system.

The limitation presented by the methodology (MA) with respect to the effect of the disturbances motivates the study of methods to take into account all input variables in the estimation of process gradients, and even Wenzel et al. (2015) tried a variant of the methodology that considers disturbances. In this paper, a method is presented that uses the past measurements and contemplates both types of input variables, namely decision variables ($\boldsymbol{u}$) and disturbances ($\boldsymbol{\xi}$), in order to obtain an accurate estimation of the gradient of the process with respect to $\boldsymbol{u}$. With this in mind, the aim is to have an optimization layer capable of reaching and maintaining the optimal conditions of the plant, in spite of changes in measured or estimated disturbances.

The remainder of this paper is organized as follows. Section 2 describes the MA methodology. Section 3 shows the extended technique that includes disturbances. Section 4 presents the application of the proposed methodology in an experimental flotation column. Section 5 exhibits the simulation and experimental results. Finally, Section 6 provides the conclusions of the paper.

2. Modifier Adaptation for Real-Time-Optimization

Due to the growing competitiveness of the process industry, it is increasingly necessary to improve the efficiency of the processes. A useful tool for that is RTO, which consists of model-based optimization that operates iteratively by taking measurements directly from the process, proposing changes in the set-points of the lower supervisory layers and bringing the plant to the economic optimum. Eq. (1) describes a model-based optimization, where $J_m \in \mathbb{R}$ is the objective function, and $\boldsymbol{C_m} \in \mathbb{R}^{n_C}$ are the inequality constraints, calculated using an available model.

$$\begin{aligned} &\min_{\boldsymbol{u}\in\boldsymbol{U}} J_m(\boldsymbol{u},\boldsymbol{\alpha}) \\ &s.t.: \\ &\boldsymbol{C_m}(\boldsymbol{u},\boldsymbol{\alpha}) \leq \boldsymbol{0} \end{aligned} \tag{1}$$

The uncertainty inherent in each model prevents the optimum determined in a model-based optimization from converging to the actual optimum of the process. Therefore, the real-time implementation should consider past measurements made to the process and its effect on the cost function and constraints.

One of the most current technologies in real-time process optimization is the RTO with Modifier Adaptation (MA) because it can manipulate modeling errors, correcting the model-based optimization using experimental gradients of the objective function and constraints. Eq. (2) explains the optimization problem in the kth iteration, which includes the modifier of the objective function $\boldsymbol{\lambda_k} \in \mathbb{R}^{n_u}$, and the modifiers $\boldsymbol{\gamma_k} \in \mathbb{R}^{n_c \times n_u}$ and $\boldsymbol{\varepsilon_k} \in \mathbb{R}^{n_c}$ of the constraints.

$$\begin{aligned} &\min_{\boldsymbol{u}\in\boldsymbol{U}} J_m(\boldsymbol{u},\boldsymbol{\alpha}) + \boldsymbol{\lambda_k^T}(\boldsymbol{u}-\boldsymbol{u_k}) \\ &s.t.: \\ &\boldsymbol{C_{mod}} \coloneqq \boldsymbol{C_m}(\boldsymbol{u},\boldsymbol{\alpha}) + \boldsymbol{\gamma_k^T}(\boldsymbol{u}-\boldsymbol{u_k}) + \boldsymbol{\varepsilon_k} \leq 0 \end{aligned} \tag{2}$$

$$\begin{aligned} \boldsymbol{\lambda_k^T} &:= \boldsymbol{\nabla_u J_p}(\boldsymbol{u_k}) - \boldsymbol{\nabla_u J_m}(\boldsymbol{u_k},\boldsymbol{\alpha}) \\ \boldsymbol{\gamma_k^T} &:= \boldsymbol{\nabla_u C_p}(\boldsymbol{u_k}) - \boldsymbol{\nabla_u C_m}(\boldsymbol{u_k},\boldsymbol{\alpha}) \\ \boldsymbol{\varepsilon_k} &:= \boldsymbol{C_p}(\boldsymbol{u_k}) - \boldsymbol{C_m}(\boldsymbol{u_k},\boldsymbol{\alpha}) \end{aligned} \tag{3}$$

In the problem shown in Eq. (2), $\boldsymbol{u_k} \in \mathbb{R}^{n_u}$ represents the actual operating point, which is calculated at the previous RTO iteration. The modifiers $\boldsymbol{\lambda_k}$, $\boldsymbol{\gamma_k}$ and $\boldsymbol{\varepsilon_k}$ are estimated from the process in the actual operating point using Eq. (3), where $J_p \in \mathbb{R}$ is the objective function and $\boldsymbol{C_p} \in \mathbb{R}^{n_C}$ are the inequality constraints; the subscript p corresponds to the process. To improve convergence, Marchetti and co-workers recommend the use of a filtering procedure of the modifiers (Marchetti et al., 2009). Eq. (4) shows these filters, where $\boldsymbol{K_\lambda}, \boldsymbol{K_\gamma}$ and $\boldsymbol{K_\varepsilon}$ represent the respective first-order filter constants for each modifier. Figure 1 summarizes the implementation of the MA methodology.

$$\begin{aligned}
\boldsymbol{\lambda_k^T} &= \boldsymbol{K_\lambda}\left(\boldsymbol{\nabla_u J_p(u_k)} - \boldsymbol{\nabla_u J_m(u_k, \alpha)}\right) + (\boldsymbol{I} - \boldsymbol{K_\lambda})\boldsymbol{\lambda_{k-1}^T} \\
\boldsymbol{\gamma_k^T} &= \boldsymbol{K_\gamma}\left(\boldsymbol{\nabla_u C_p(u_k)} - \boldsymbol{\nabla_u C_m(u_k, \alpha)}\right) + (\boldsymbol{I} - \boldsymbol{K_\gamma})\boldsymbol{\gamma_{k-1}^T} \\
\boldsymbol{\varepsilon_k} &= \boldsymbol{K_\varepsilon}\left(\boldsymbol{C_p(u_k)} - \boldsymbol{C_m(u_k, \alpha)}\right) + (\boldsymbol{I} - \boldsymbol{K_\varepsilon})\boldsymbol{\varepsilon_{k-1}^T}
\end{aligned} \tag{4}$$

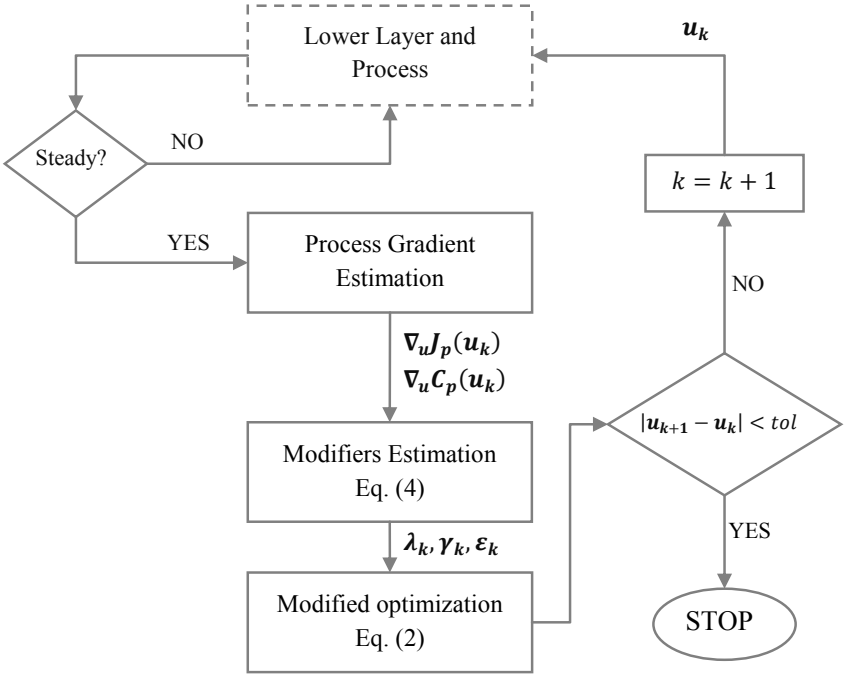

Figure 1. Implementation algorithm of the modifier-adaptation methodology.

Furthermore, according to Marchetti and co-workers, the Karush-Kuhn-Tucker (KKT) conditions of the modified model match the conditions of the real process (Marchetti et al., 2010). This implies that if second-order conditions hold at this point, and then, it is possible to find the local optimum of the real plant through solving the modified problem. Eq. (5) describes the Necessary Optimality Conditions (NOC) of the modified problem.

$$\begin{aligned}
\boldsymbol{\nabla_u \mathcal{L}_{mod}(u_{k+1}, \alpha)} &\coloneqq \boldsymbol{\nabla_u J_m(u_{k+1}, \alpha)} + \boldsymbol{\lambda_k^T} + \boldsymbol{\mu^T}\left(\boldsymbol{\nabla_u C_m(u_{k+1}, \alpha)} + \boldsymbol{\gamma_k^T}\right) = \boldsymbol{0} \\
\boldsymbol{C_{mod}(u_{k+1}, \alpha)} &= \boldsymbol{C_m(u_{k+1}, \alpha)} + \boldsymbol{\gamma_k^T(u_{k+1} - u_k)} + \boldsymbol{\varepsilon_k} \leq \boldsymbol{0}
\end{aligned} \tag{5}$$

$$\boldsymbol{\mu} \geq \mathbf{0}$$
$$C_{mod}^{j}(\boldsymbol{u_{k+1}}, \boldsymbol{\alpha}) \cdot \mu^{j} = 0, \qquad j = 1 \dots n_C$$

Under the assumption of convergence, $\boldsymbol{u_k} \rightarrow \boldsymbol{u}_\infty$, and taking into account the definitions of the modifiers, the optimality conditions are restated as Eq. (6), which represents the NOC of the real process.

$$\begin{aligned}
&\boldsymbol{\nabla_u \mathcal{L}_{mod}}(\boldsymbol{u}_\infty, \boldsymbol{\alpha}) = \boldsymbol{\nabla_u \mathcal{L}_p}(\boldsymbol{u}_\infty) = \boldsymbol{\nabla_u J_p}(\boldsymbol{u}_\infty) + \boldsymbol{\mu}^{\boldsymbol{T}} \left(\boldsymbol{\nabla_u C_p}(\boldsymbol{u}_\infty)\right) = \mathbf{0} \\
&\boldsymbol{C_{mod}}(\boldsymbol{u}_\infty, \boldsymbol{\alpha}) = \boldsymbol{C_p}(\boldsymbol{u}_\infty) \leq 0 \\
&\boldsymbol{\mu} \geq \mathbf{0} \\
&C_p^j(\boldsymbol{u}_\infty) \cdot \mu^j = 0, \; j = 1 \dots n_C
\end{aligned} \tag{6}$$

2.1. Gradient estimation

In the real-time optimization problems with modifier adaptation, different methodologies have been proposed for changing the gradient estimation step, which influences the computation of modifiers.

2.1.1. Finite Differences

This method consists of perturbing the system around the current point of operation, changing just one decision variable and recording the outputs of the process (Roberts, 1979). When all perturbations are ready, the next stage of the RTO layer can be advanced (see Figure 1). Navia et al. (2016) implemented the experimental equipment used in this work. It has been shown to be an inefficient method for slow dynamic processes (Mansour & Ellis, 2003).

2.1.2. Dual control optimization

This approach consists of the use of past measurements for the estimation of gradients. Therefore, it should ensure that the collected measures have sufficient energy for that evaluation, adding another restriction to the optimization problem (Brdys & Tatjewski, 1994). The name "dual" comes from the additional constraint that must be added to the modified problem, to guarantee identifiability of process curvatures in the next RTO iteration. In this work, the rank-one update based on an approximation of the directional derivatives is used, which was proposed by Brdys & Tatjewski (1994). Eq. (7) shows the process gradient estimation, where the matrix $\boldsymbol{S_k}$ is square and non-singular, formed by the linearly independent $\boldsymbol{s_{k,i}}$ elements, which are defined as the differences between the current decision variables and the previous ones.

$$\begin{aligned}
&\boldsymbol{\nabla_u y^j_{p_k}} \approx (\boldsymbol{S_k})^{-1} \boldsymbol{\psi^j_k}, \qquad j = 1 \dots n_C + 1 \\
&\boldsymbol{y_p} \coloneqq \left[J_p, \boldsymbol{C_p}\right]^T \\
&\boldsymbol{S_k} = [\boldsymbol{s_{k,1}} \quad \cdots \quad \boldsymbol{s_{k,n_u}}]^T, \qquad \boldsymbol{s_{k,i}} \coloneqq \boldsymbol{u_k} - \boldsymbol{u_{k-i}}, \quad i = 1, \dots, n_u \\
&\boldsymbol{\psi^j_k} = \left[\Delta y^j_{p\,k,1} \quad \cdots \quad \Delta y^j_{p\,k,n_u}\right]^T, \quad \Delta y^j_{p\,k,i} \coloneqq y^j_p(\boldsymbol{u_k}) - y^j_p(\boldsymbol{u_{k-i}}), \quad i = 1, \dots, n_u
\end{aligned} \tag{7}$$

In Eq. (7), $\boldsymbol{\nabla_u y^j_{p_k}}$ is the gradient of process variable y_p^j with respect to decision variables $\boldsymbol{u}$, evaluated at k[th] RTO iteration.

Although this methodology presents advantages with respect to the convergence time, it is necessary to add the dual constraint for $\boldsymbol{S_{k+1}}$ to the modified problem, to ensure identifiability. Eq. (8) shows this restriction, where the inverse of the condition number $\kappa(\cdot)$ of matrix $\boldsymbol{S_{k+1}}$, must be greater than a given limit δ_L.

$$\kappa(\boldsymbol{S_{k+1}}) \geq \delta_L \tag{8}$$

This additional constraint reduces the feasible region for the original modified problem, which implies a loss of optimality in the RTO iteration that some authors justify regarding the possibility to estimate the gradient of the process accurately (Brdys & Tatjewski, 2005; Marchetti et al., 2010). As already mentioned, in this work we have used this approach to extend the methodology to cases when disturbances can be measured or estimated.

2.1.3. Nested modified adaptation

The estimation of the process gradients implies having a continually excited system, which could cause operational problems. With this in mind, Navia and co-workers have proposed a reformulation of modifier adaptation as a nested optimization problem called the Nested Modified Adaptation (NMA) (Navia et al., 2015). NMA follows a similar structure as the original method, but it replaces the estimation of the gradient modifiers λ_k and γ_k for an upper optimization layer.

2.1.4. Quadratic approximation of data collected

Gao et al. (2016) have proposed a methodology that, unlike other methods, use $n_u + 1$ measurements, it uses all measures obtained to perform a regression with a quadratic function of data previously chosen. Then, the gradients can be estimated analytically from this adjusted curve.

2.1.5. Using transient information

Two methods have arisen to increase the speed of convergence of the RTO layer, especially when dealing with slow dynamic processes.

First, François & Bonvin (2013) presented a gradient estimation method using transient information for steady-state optimization, although the gradients are defined only at steady state.

Later, Rodríguez-Blanco et al. (2017) presented another methodology that proposed the use of transient information for the gradient estimations, based on the use of a truncated Taylor expansion for the output variables combined with the least squares algorithm (RELS).

As discussed above, several methods have been developed for improving the convergence of MA. However, no technique includes handling explicitly the available information of disturbances that can be measured or estimated in processes, which can affect the NOC of the real system.

This work presents an application of the MA methodology including changes in the quantification of the experimental gradients. Considering that, most processes have several input variables, which can generate changes in the system, apart from the decision variables. Therefore, if this information is not considered, it may lead to a miscalculation of process curvature, which could mean a wrong detection of the NOC for a real system.

3. MA with disturbances

3.1. The effect of disturbances on the Modifier Adaptation Method

As mentioned above, a real system has several inputs and outputs. **Figure 2** shows a diagram that exemplifies this situation and allows relating the dependence of the outputs with respect to the inputs.

Figure 2. A general process scheme.

where:

$$\boldsymbol{y_p} = \boldsymbol{f}(\boldsymbol{u}, \boldsymbol{\xi}),\ \boldsymbol{y_p} \coloneqq [J_p, \boldsymbol{C_p}]^{\boldsymbol{T}}$$

$\boldsymbol{u} \in \mathbb{R}^{n_u}$: decision variables

$\boldsymbol{\xi} \in \mathbb{R}^{n_\xi}$: disturbances

In practice, it is difficult to block the effect of an uncontrolled variable on the response. Thus, the implementation of an RTO layer using MA should include the impact of $\boldsymbol{\xi}$ in $\boldsymbol{y_p}$ if it is available.

Expressing the measured changes in the output of the system at the k[th] iteration and using a first-order Taylor approximation as shown in Eq. (9), the variations in the output do not depend only on the changes of decision variables $\boldsymbol{u}$ *but also* on the changes in disturbances $\boldsymbol{\xi}$.

$$\Delta y_{p\,k,i}^{j} = \Delta \boldsymbol{u}_{\boldsymbol{k,i}}^{\boldsymbol{T}} \boldsymbol{\nabla_u y_{p_k}^{j}} + \Delta \boldsymbol{\xi}_{\boldsymbol{k,i}}^{\boldsymbol{T}} \boldsymbol{\nabla_\xi y_{p_k}^{j}} + \boldsymbol{\mathcal{O}^2},\ j = 1 \dots n_C + 1 \tag{9}$$

Where $\Delta \boldsymbol{\xi_{k,i}} \coloneqq \boldsymbol{\xi_k} - \boldsymbol{\xi_{k-i}}$ and $\Delta \boldsymbol{u_{k,i}} \coloneqq \boldsymbol{u_k} - \boldsymbol{u_{k-i}}$ with $i = 1, \dots, n_u$.

Using a gradient estimation method based only on the past information of $\boldsymbol{y_p}$ and $\boldsymbol{u}$, leads to an expression that only in particular cases corresponds to $\boldsymbol{\nabla_u y_{p,j}}$.

Consider, as an example, the directional derivatives approach. If we apply Eq. (9), neglecting higher order derivatives to the differences of y_p^j with respect to the previous n_u operating points, we obtain Eq. (10).

$$\boldsymbol{\psi_k^j} = \boldsymbol{S_k} \boldsymbol{\nabla_u y_{p_k}^{j}} + \boldsymbol{\Xi_k} \boldsymbol{\nabla_\xi y_{p_k}^{j}},\ j = 1 \dots n_C + 1 \tag{10}$$

where $\boldsymbol{\psi_k^j} = \left[\Delta y_{p\,k,1}^{j} \quad \cdots \quad \Delta y_{p\,k,n}^{j}\right]^T$, and $\boldsymbol{\Xi_k} \coloneqq [\boldsymbol{\Delta \xi_{k,1}} \quad \cdots \quad \boldsymbol{\Delta \xi_{k,n_u}}]^{\boldsymbol{T}}$.

Pre-multiplying Eq. (10) by $\boldsymbol{S_k^{-1}}$ (assuming that it is not singular), we get Eq. (11).

$$\boldsymbol{\nabla_u y_{p_k}^j = S_k^{-1} \psi_k^j - S_k^{-1} \Xi_k \nabla_\xi y_{p_k}^j},\ j = 1 \dots n_C + 1 \tag{11}$$

The first term on the right-hand side of Eq. (11) is the estimation of the gradient using the directional derivative approach from Eq. (7), which is only equal to $\boldsymbol{\nabla_u y_{p_k}^j}$ under two possible scenarios: (1) there are no variations in $\boldsymbol{\xi}$ during the last n_u operating points; or (2) disturbances do not affect $\boldsymbol{y_p}$. In other cases, the information of changes in the disturbances must be considered to estimate the process curvature accurately with respect to the decision variables. To visualize the effect of this miscalculation, it is assumed that the MA methodology converges, and it is considered that neither scenario 1 nor 2 are satisfied. Replacing the estimation of the process gradient using directional derivatives into the stationarity condition of the modified problem leads to Eq. (12), which is not the KKT point of the process. Therefore, it is possible to say that neglecting the information of disturbances in the process gradient calculation can compromise the ability to find the NOC of the process.

$$\begin{aligned}\boldsymbol{\nabla_u \mathcal{L}_{mod}} = \boldsymbol{\nabla_u J_p(u_\infty, \xi_\infty) + S_\infty^{-1} \Xi_\infty \nabla_\xi J_p(u_\infty, \xi_\infty) + \mu^T \Big(\nabla_u C_p(u_\infty, \xi_\infty) +} \\ \boldsymbol{S_\infty^{-1} \Xi_\infty \nabla_\xi C_p(u_\infty, \xi_\infty) \Big) = 0}\end{aligned} \tag{12}$$

A similar analysis can be done for other gradient estimation methods that only consider past information of $\boldsymbol{y_p}$ and $\boldsymbol{u}$. Then, it is necessary to take into account processes where the disturbances affect the outputs, changing $\boldsymbol{\xi}$ in every iteration, in order to estimate the process derivatives accurately.

3.2. Proposed Extension of the Dual Methodology

In this work, we propose the extension of the dual methodology for gradient estimation to take into account explicitly the available information of $\boldsymbol{\xi}$, assuming that these variables can be measured or estimated. As a remark, other alternatives can be investigated, such as increasing the energy of matrix $\boldsymbol{S_k}$ to make the changes in decision variables more important than the changes in the disturbances. However, precautions are needed since this can compromise the gradient estimation due to the distance between the previous values of $\boldsymbol{u}$ from the actual one.

The proposed method has a similar implementation structure as the one shown in Figure 1, but the stage of gradient estimation corresponds to the use of the extended dual methodology, since it also considers the measured or estimated changes in the disturbances. Applying the Taylor expansion of Eq. (9) is necessary in order to calculate the experimental gradients, using the differences of the actual measurements with respect to the $n = n_u + n_\xi$ previous operating points, as Eq. (13) shows.

$$\boldsymbol{\psi_k^j \approx \bar{S}_k \nabla_{\bar{u}} y_{p_k}^j},\ j = 1 \dots n_C + 1 \tag{13}$$

where $\overline{\boldsymbol{u}} \coloneqq [\boldsymbol{u}, \boldsymbol{\xi}]^T$, $\overline{\boldsymbol{S}}_{\boldsymbol{k}} \coloneqq [\overline{\boldsymbol{s}}_{\boldsymbol{k},\boldsymbol{1}} \quad \cdots \quad \overline{\boldsymbol{s}}_{\boldsymbol{k},\boldsymbol{n}}]^T$, $\overline{\boldsymbol{s}}_{\boldsymbol{k},\boldsymbol{i}} = \overline{\boldsymbol{u}}_{\boldsymbol{k}} - \overline{\boldsymbol{u}}_{\boldsymbol{k}-\boldsymbol{i}}$, and $\boldsymbol{\psi}_{\boldsymbol{k}}^{\boldsymbol{j}} = \left[\Delta \boldsymbol{y}_{\boldsymbol{p}}{}^{j}_{k,1} \quad \ldots \quad \Delta \boldsymbol{y}_{\boldsymbol{p}}{}^{j}_{k,n}\right]^T$. Under the assumption that $\overline{\boldsymbol{S}}_{\boldsymbol{k}}$ is nonsingular, the gradient of process variable $\boldsymbol{y}_{\boldsymbol{p}}^{\boldsymbol{j}}$ with respect to input variables can be obtained from Eq. (14).

$$\boldsymbol{\nabla}_{\overline{\boldsymbol{u}}} \boldsymbol{y}_{\boldsymbol{k}}^{\boldsymbol{j}} \approx (\overline{\boldsymbol{S}}_{\boldsymbol{k}})^{-1} \boldsymbol{\psi}_{\boldsymbol{k}}^{\boldsymbol{j}},\ j = 1 \ldots n_C + 1 \tag{14}$$

To ensure identifiability, an additional constraint must be added to the modified optimization problem, as Eq. (15) shows.

$$\begin{aligned} &\min_{\boldsymbol{u} \in \boldsymbol{U}} J_m(\boldsymbol{u}, \boldsymbol{\alpha}) + \boldsymbol{\lambda}_{\boldsymbol{k}}^{\boldsymbol{T}}(\boldsymbol{u} - \boldsymbol{u}_{\boldsymbol{k}}) \\ &s.t.: \\ &\boldsymbol{C}_{\boldsymbol{m}}(\boldsymbol{u}, \boldsymbol{\alpha}) + \boldsymbol{\gamma}_{\boldsymbol{k}}^{\boldsymbol{T}}(\boldsymbol{u} - \boldsymbol{u}_{\boldsymbol{k}}) + \boldsymbol{\varepsilon}_{\boldsymbol{k}} \leq 0 \\ &|(\boldsymbol{u} - \boldsymbol{u}_{\boldsymbol{k}})^T \boldsymbol{w}_{\boldsymbol{k}} + (\boldsymbol{\xi}_{\boldsymbol{k+1}} - \boldsymbol{\xi}_{\boldsymbol{k}})^T \boldsymbol{\vartheta}_{\boldsymbol{k}}| \geq \delta \end{aligned} \tag{15}$$

where $\boldsymbol{w}_{\boldsymbol{k}} \in \mathbb{R}^{n_u}$ and $\boldsymbol{\vartheta}_{\boldsymbol{k}} \in \mathbb{R}^{n_\xi}$ are the component vectors of $\boldsymbol{\pi}_{\boldsymbol{k}} \coloneqq [\boldsymbol{w}_{\boldsymbol{k}}, \boldsymbol{\vartheta}_{\boldsymbol{k}}]^{\boldsymbol{T}}$, which is the vector orthonormal to the subspace $V_k = \langle \{\overline{\boldsymbol{s}}_{\boldsymbol{k},\boldsymbol{1}}, \ldots, \overline{\boldsymbol{s}}_{\boldsymbol{k},\boldsymbol{n-1}}\} \rangle$, and δ is greater than zero.

As the value of $\boldsymbol{\xi}_{\boldsymbol{k+1}}$ is unknown when the RTO is solved, this must be estimated from available models using previously determined values. Once the system reaches the steady state, the dual constraint must be reevaluated with the measured or estimated value of $\boldsymbol{\xi}_{\boldsymbol{k}}$. Since matrix $\overline{\boldsymbol{S}}_{\boldsymbol{k}}$ has an independent part, it is necessary to evaluate the cases of $\boldsymbol{\xi}$ when identifiability problems may arise. Section 3.3 presents a theorem to give sufficient conditions for linear independency of matrix $\overline{\boldsymbol{S}}_{\boldsymbol{k+1}}$.

Figure 3 summarizes the implementation algorithm for the proposed methodology which is detailed below:

Algorithm

Step 0: Set $k = 0$ and initialize $\boldsymbol{u}_{\boldsymbol{k}}$, $\boldsymbol{\lambda}_{\boldsymbol{k}}$, $\boldsymbol{\gamma}_{\boldsymbol{k}}$ and $\boldsymbol{\varepsilon}_{\boldsymbol{k}}$. Calculate and apply $\boldsymbol{u}_{\boldsymbol{k}}$ into the process. This value can be obtained by solving the model-based optimization, or by using other operational criteria. Wait until steady state to estimate $J_{p,k}$, $\boldsymbol{C}_{\boldsymbol{p},\boldsymbol{k}}$ and $\boldsymbol{\xi}_{\boldsymbol{k}}$ from the available data. Set $k = k + 1$ and repeat the application for another value for $\boldsymbol{u}_{\boldsymbol{k}}$ in the process up to $k = n + 1$, such that the matrix $\overline{\boldsymbol{S}}_{\boldsymbol{k}}$ is invertible. To do so, the changes in $\boldsymbol{u}_{\boldsymbol{k}}$ can be chosen to be orthogonal among them, or it can be added a random component in the changes for avoiding linear dependency.

For every $k \geq n + 1$:

Step 1: Measure or estimate $\boldsymbol{\xi}_{\boldsymbol{k}}$ and calculate $\boldsymbol{\pi}_{\boldsymbol{k-1}}$. Check whether or not the dual constraint $|(\boldsymbol{u}_{\boldsymbol{k}} - \boldsymbol{u}_{\boldsymbol{k-1}})^T \boldsymbol{w}_{\boldsymbol{k-1}} + (\boldsymbol{\xi}_{\boldsymbol{k}} - \boldsymbol{\xi}_{\boldsymbol{k-1}})^T \boldsymbol{\vartheta}_{\boldsymbol{k-1}}| \geq \delta$ is fulfilled; if this is the case, then go to Step 2. Otherwise, if there are components of vector $\boldsymbol{\xi}_{\boldsymbol{k}}$ that have not changed between k and $k - 1$ (i.e., $\xi_k^j = \xi_{k-1}^j, \forall j \in \Gamma$, where Γ is the set of the n_J unchanged perturbations), then remove these elements from the matrix $\overline{\boldsymbol{S}}_{\boldsymbol{k}}$ and go to Step 2. If this is not the case, linear dependencies of elements of $\boldsymbol{\xi}$ are produced, so it is

necessary to wait for changes in $\boldsymbol{\xi}$ that satisfies dual constraint. Notice that $|(\boldsymbol{u_k} - \boldsymbol{u_{k-1}})^T \boldsymbol{w_{k-1}} + (\boldsymbol{\xi_k} - \boldsymbol{\xi_{k-1}})^T \boldsymbol{\vartheta_{k-1}}| \geq \delta$ is the dual constraint from Eq. (15), applied to the actual operating point. The fulfillment of this condition must be evaluated because when Eq. (15) was solved, $\boldsymbol{\xi_{k+1}}$ had been estimated using past values of disturbances.

Step 2: Estimate the gradients of the model and the process according to Eq. (14), extracting $\boldsymbol{\nabla_u J}$ and $\boldsymbol{\nabla_u C}$, and calculate the modifiers according to Eq. (4) in Section 2.1.

Step 3: Solve the modified optimization problem to obtain $\boldsymbol{u_{k+1}}$, according to Eq. (15). Compare the dependence of the convergence criterion, and if it is satisfied, then it stops. Otherwise, set $k = k + 1$, apply $\boldsymbol{u_k}$ to the process, wait until steady state, and go to Step 1.

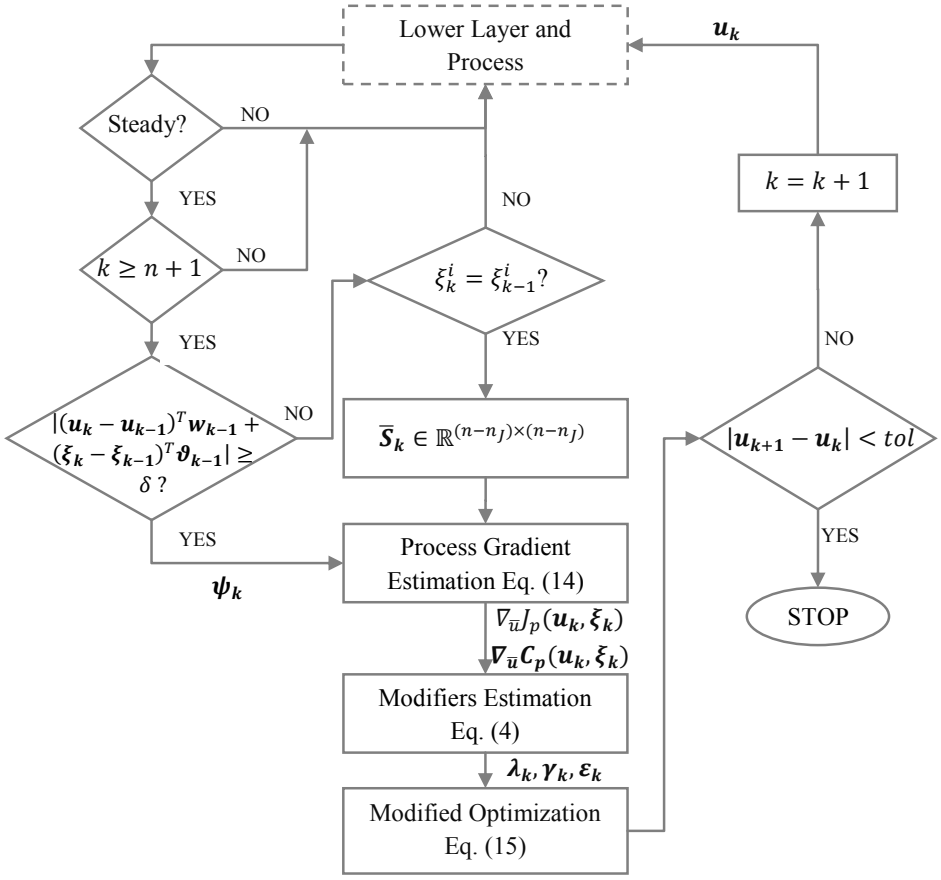

Figure 3. Implementation of the proposed extension of the modifier-adaptation method.

3.3 Sufficient conditions of invertibility for matrix $\bar{S}_k$

Let n_u, n_ξ and $n = n_u + n_\xi$, natural numbers corresponding to the dimensions of vectors $\boldsymbol{u}$, $\boldsymbol{\xi}$ and $\boldsymbol{s}$, respectively, and $k \in \mathbb{N}$ the iteration number of the method. For every $k \geq n$ and vectors $\boldsymbol{u_{k-n}}, \dots, \boldsymbol{u_k} \in \mathbb{R}^{n_u}$ and $\boldsymbol{\xi_{k-n}}, \dots, \boldsymbol{\xi_k} \in \mathbb{R}^{n_\xi}$, we define

$$\Delta \boldsymbol{u_{k,i}} \coloneqq \boldsymbol{u_k} - \boldsymbol{u_{k-i}}, \qquad \Delta \boldsymbol{\xi_{k,i}} \coloneqq \boldsymbol{\xi_k} - \boldsymbol{\xi_{k-i}}, \qquad \bar{\boldsymbol{s}}_{\boldsymbol{k,i}} = \begin{pmatrix} \Delta \boldsymbol{u_{k,i}} \\ \Delta \boldsymbol{\xi_{k,i}} \end{pmatrix} \quad \forall\, i = 1, \dots, n.$$

Then, the problem to solve is the following:

Problem 1: Suppose that $\bar{\boldsymbol{s}}_{\boldsymbol{k,1}}, \dots, \bar{\boldsymbol{s}}_{\boldsymbol{k,n}}$ are linearly independent. Given $\Delta \boldsymbol{\xi_{k+1,1}} \in \mathbb{R}^{n_\xi}$, it is necessary to find $\Delta \boldsymbol{u_{k+1,1}} \in \mathbb{R}^{n_u}$ (if it exists) such that the vectors

$$\bar{\boldsymbol{s}}_{\boldsymbol{k+1,1}}, \bar{\boldsymbol{s}}_{\boldsymbol{k+1,2}}, \dots, \bar{\boldsymbol{s}}_{\boldsymbol{k+1,n}}$$

are linearly independent.

To solve the problem, first we have to relate the new vectors to the old ones that we already know are linearly independent. To do so, note that

$$\bar{\boldsymbol{s}}_{\boldsymbol{k+1,i}} = \bar{\boldsymbol{s}}_{\boldsymbol{k+1,1}} + \bar{\boldsymbol{s}}_{\boldsymbol{k,i-1}}, \quad \forall\, i = 2, \dots, n. \tag{16}$$

Proposition: $\bar{\boldsymbol{s}}_{\boldsymbol{k+1,1}}, \bar{\boldsymbol{s}}_{\boldsymbol{k,1}}, \dots, \bar{\boldsymbol{s}}_{\boldsymbol{k,n-1}}$ are linearly independent if and only if $\bar{\boldsymbol{s}}_{\boldsymbol{k+1,1}}, \bar{\boldsymbol{s}}_{\boldsymbol{k+1,2}}, \dots, \bar{\boldsymbol{s}}_{\boldsymbol{k+1,n}}$ are linearly independent.

Proof. Let $\alpha_1, \dots, \alpha_n \in \mathbb{R}$ such that $\sum_{i=1}^{n} \alpha_i \bar{\boldsymbol{s}}_{\boldsymbol{k+1,i}} = 0$. We want to demonstrate, using the hypothesis, that $\alpha_1 = \cdots = \alpha_n = 0$. Using Eq. (16), we obtain

$$\begin{aligned} 0 = \alpha_1 \bar{\boldsymbol{s}}_{\boldsymbol{k+1,1}} + \sum_{i=2}^{n} \alpha_i \bar{\boldsymbol{s}}_{\boldsymbol{k+1,i}} &= \alpha_1 \bar{\boldsymbol{s}}_{\boldsymbol{k+1,1}} + \left(\sum_{i=2}^{n} \alpha_i \right) \bar{\boldsymbol{s}}_{\boldsymbol{k+1,1}} + \sum_{i=2}^{n} \alpha_i \bar{\boldsymbol{s}}_{\boldsymbol{k,i-1}} \\ &= \left(\sum_{i=1}^{n} \alpha_i \right) \bar{\boldsymbol{s}}_{\boldsymbol{k+1,1}} + \sum_{j=1}^{n-1} \alpha_{j+1} \bar{\boldsymbol{s}}_{\boldsymbol{k,j}} \end{aligned}$$

As by hypothesis $\bar{\boldsymbol{s}}_{\boldsymbol{k+1,1}}, \bar{\boldsymbol{s}}_{\boldsymbol{k,1}}, \dots, \bar{\boldsymbol{s}}_{\boldsymbol{k,n-1}}$ are linearly independent, we have $\sum_{i=1}^{n} \alpha_i = 0$ and $\alpha_2 = \cdots = \alpha_n = 0$, where the result is concluded. For the reciprocal, let $\alpha_1, \dots, \alpha_n \in \mathbb{R}$ such that $\sum_{i=1}^{n-1} \alpha_i \bar{\boldsymbol{s}}_{\boldsymbol{k,i}} + \alpha_n \bar{\boldsymbol{s}}_{\boldsymbol{k+1,1}} = 0$. Using again Eq. (16), we obtain

$$\begin{aligned} 0 = \alpha_n \bar{\boldsymbol{s}}_{\boldsymbol{k+1,1}} + \sum_{i=2}^{n} \alpha_{i-1} \bar{\boldsymbol{s}}_{\boldsymbol{k,i-1}} &= \alpha_n \bar{\boldsymbol{s}}_{\boldsymbol{k+1,1}} + \sum_{i=2}^{n} \alpha_{i-1} \bar{\boldsymbol{s}}_{\boldsymbol{k+1,i}} - \left(\sum_{i=2}^{n} \alpha_{i-1} \right) \bar{\boldsymbol{s}}_{\boldsymbol{k+1,1}} \\ &= \left(\alpha_n - \sum_{i=1}^{n-1} \alpha_i \right) \bar{\boldsymbol{s}}_{\boldsymbol{k+1,1}} + \sum_{i=2}^{n} \alpha_{i-1} \bar{\boldsymbol{s}}_{\boldsymbol{k+1,i}} \end{aligned}$$

as $\bar{\boldsymbol{s}}_{\boldsymbol{k+1,1}}, \bar{\boldsymbol{s}}_{\boldsymbol{k+1,2}}, \dots, \bar{\boldsymbol{s}}_{\boldsymbol{k+1,n}}$ are linearly independent, we have $\alpha_n - \sum_{i=1}^{n-1} \alpha_i = 0$ and $\alpha_1 = \cdots = \alpha_{n-1} = 0$.

The previous proposition tell us that the Problem 1 is equivalent to

Problem 2: Suppose that $\bar{\boldsymbol{s}}_{\boldsymbol{k,1}}, \dots, \bar{\boldsymbol{s}}_{\boldsymbol{k,n}}$ are linearly independent. Given $\Delta\boldsymbol{\xi}_{\boldsymbol{k+1,1}} \in \mathbb{R}^{n_\xi}$, it is necessary to find $\Delta\boldsymbol{u}_{\boldsymbol{k+1,1}} \in \mathbb{R}^{n_u}$ (if it exists) such that

$$\bar{\boldsymbol{s}}_{\boldsymbol{k+1,1}}, \bar{\boldsymbol{s}}_{\boldsymbol{k,1}}, \dots, \bar{\boldsymbol{s}}_{\boldsymbol{k,n-1}}$$

are linearly independent.

The advantage of this new formulation of the problem is that $\bar{\boldsymbol{s}}_{\boldsymbol{k,1}}, \dots, \bar{\boldsymbol{s}}_{\boldsymbol{k,n-1}}$ only have information from the iteration k backwards, so they do not depend on $\bar{\boldsymbol{s}}_{\boldsymbol{k+1}}$.

Theorem 1. Given $k \geq n$, let $\boldsymbol{\pi}_{\boldsymbol{k}} \in \mathbb{R}^n \setminus \{0\}$ the vector normal to subspace $\mathbb{R}^n$ generated by $\bar{\boldsymbol{s}}_{\boldsymbol{k,1}}, \dots, \bar{\boldsymbol{s}}_{\boldsymbol{k,n-1}}$, i.e., $\boldsymbol{V}_{\boldsymbol{k}} = \langle\{\bar{\boldsymbol{s}}_{\boldsymbol{k,1}}, \dots, \bar{\boldsymbol{s}}_{\boldsymbol{k,n-1}}\}\rangle$. Let us denote $\boldsymbol{\pi}_{\boldsymbol{k}} = \begin{pmatrix} \boldsymbol{w}_{\boldsymbol{k}} \\ \boldsymbol{\vartheta}_{\boldsymbol{k}} \end{pmatrix}$, where $\boldsymbol{w}_{\boldsymbol{k}} \in \mathbb{R}^{n_u}$ and $\boldsymbol{\vartheta}_{\boldsymbol{k}} \in \mathbb{R}^{n_\xi}$. Then, if $\boldsymbol{w}_{\boldsymbol{k}} \neq 0$, for every $\Delta\boldsymbol{\xi}_{\boldsymbol{k+1,1}} \in \mathbb{R}^{n_\xi}$, there exists $\Delta\boldsymbol{u}_{\boldsymbol{k+1,1}} \in \mathbb{R}^{n_u}$ such that $\bar{\boldsymbol{s}}_{\boldsymbol{k+1,1}}$ is linearly independent with respect to $\boldsymbol{V}_{\boldsymbol{k}}$, i.e., $\bar{\boldsymbol{s}}_{\boldsymbol{k+1,1}}, \bar{\boldsymbol{s}}_{\boldsymbol{k,1}}, \dots, \bar{\boldsymbol{s}}_{\boldsymbol{k,n-1}}$ are linearly independent. It can be found by ensuring $\left|\left(\Delta\boldsymbol{u}_{\boldsymbol{k+1,1}}\right)^T \boldsymbol{w}_{\boldsymbol{k}} + \left(\Delta\boldsymbol{\xi}_{\boldsymbol{k+1,1}}\right)^T \boldsymbol{\vartheta}_{\boldsymbol{k}}\right| \geq \delta > 0$.

Proof. Indeed, since $\bar{\boldsymbol{s}}_{\boldsymbol{k,1}}, \dots, \bar{\boldsymbol{s}}_{\boldsymbol{k,n-1}}$ are linearly independent, $\boldsymbol{V}_{\boldsymbol{k}}$ is an $n-1$-dimensional subspace of $\mathbb{R}^n$ and there exists $\boldsymbol{\pi}_{\boldsymbol{k}} = \begin{pmatrix} \boldsymbol{w}_{\boldsymbol{k}} \\ \boldsymbol{\vartheta}_{\boldsymbol{k}} \end{pmatrix} \in \mathbb{R}^n \setminus \{0\}$ which is normal to $\boldsymbol{V}_{\boldsymbol{k}}$. Therefore, $\boldsymbol{B} = \left\{\bar{\boldsymbol{s}}_{\boldsymbol{k,1}}, \dots, \bar{\boldsymbol{s}}_{\boldsymbol{k,n-1}}, \boldsymbol{\pi}_{\boldsymbol{k}}\right\}$ is a basis of $\mathbb{R}^n$.

Note that, for every $\bar{\boldsymbol{s}} \in \mathbb{R}^n$ we have $\bar{\boldsymbol{s}} \in \boldsymbol{V}$ if and only if $\bar{\boldsymbol{s}}^T \boldsymbol{\pi}_{\boldsymbol{k}} = 0$. Indeed, since $\boldsymbol{B}$ is a basis of $\mathbb{R}^n$, exist $a_1, \dots, a_{n-1}, a \in \mathbb{R}$, such that $\bar{\boldsymbol{s}} = \sum_{i=1}^{n-1} a_i \bar{\boldsymbol{s}}_{\boldsymbol{k,i}} + a\boldsymbol{\pi}_{\boldsymbol{k}}$ and then $\bar{\boldsymbol{s}}^T \boldsymbol{\pi}_{\boldsymbol{k}} = \sum_{i=1}^{n-1} a_i \bar{\boldsymbol{s}}_{\boldsymbol{k,i}}{}^T \boldsymbol{\pi}_k + a|\boldsymbol{\pi}_{\boldsymbol{k}}|^2 = a|\boldsymbol{\pi}_{\boldsymbol{k}}|^2$, which is equal to 0 if and only if $a = 0$ or, equivalently, $\bar{\boldsymbol{s}} \in \boldsymbol{V}_{\boldsymbol{k}}$.

Therefore, given $\Delta\boldsymbol{\xi}_{\boldsymbol{k+1,1}} \in \mathbb{R}^{n_\xi}$, for obtaining that $\bar{\boldsymbol{s}}_{\boldsymbol{k+1,1}}$ is linearly independent to $\boldsymbol{V}_{\boldsymbol{k}}$ it is enough to find $\Delta\boldsymbol{u}_{\boldsymbol{k+1,1}} \in \mathbb{R}^{n_u}$ such that $0 \neq \bar{\boldsymbol{s}}_{\boldsymbol{k+1,1}}{}^T \boldsymbol{\pi}_{\boldsymbol{k}} = \Delta\boldsymbol{u}_{\boldsymbol{k+1,1}}{}^T \boldsymbol{w}_{\boldsymbol{k}} + \Delta\boldsymbol{\xi}_{\boldsymbol{k+1,1}}{}^T \boldsymbol{\vartheta}_{\boldsymbol{k}}$, which is always possible to find if $\boldsymbol{w}_{\boldsymbol{k}} \neq 0$.

Theorem 1 gives conditions for the existence of a solution to Problem 2. The next result characterizes those conditions.

Proposition 2. Under the previous notation, we have $\boldsymbol{w}_{\boldsymbol{k}} = 0$ if and only if $\dim\left(Im\left[\Delta\boldsymbol{\xi}_{\boldsymbol{k,1}} | \dots | \Delta\boldsymbol{\xi}_{\boldsymbol{k,n-1}}\right]\right) < n_\xi$

Proof. Indeed, if $\boldsymbol{w}_{\boldsymbol{k}} = 0$ then the orthogonality condition $\bar{\boldsymbol{s}}_{\boldsymbol{k,i}}^T \boldsymbol{\pi}_{\boldsymbol{k}} = 0$, for every $i = 1, \dots, n-1$ reads $\Delta\boldsymbol{\xi}_{\boldsymbol{k,i}}{}^T \boldsymbol{\vartheta}_{\boldsymbol{k}} = 0, \ \forall i = 1, \dots, n-1$, where $\boldsymbol{\vartheta}_{\boldsymbol{k}} \neq 0$. Equivalently, $\boldsymbol{\vartheta}_{\boldsymbol{k}} \in Ker\Xi$, where

$$\Xi = \begin{bmatrix} \Delta\boldsymbol{\xi}_{\boldsymbol{k,1}}{}^T \\ \vdots \\ \Delta\boldsymbol{\xi}_{\boldsymbol{k,n-1}}{}^T \end{bmatrix} \in \mathbb{R}^{(n-1)\times n_\xi}$$

which yields $\dim(Ker\ \Xi) \geq 1$. Therefore, since $Ker\ \Xi + \mathrm{Im}\ \Xi^T = \mathbb{R}^{n_\xi}$, then $\dim\left(Im\left[\Delta\boldsymbol{\xi}_{\boldsymbol{k,n}}|\ldots|\Delta\boldsymbol{\xi}_{\boldsymbol{k,1}}\right]\right) \leq n_\xi - 1$. Conversely, if $\dim\left(Im\left[\Delta\boldsymbol{\xi}_{\boldsymbol{k,n}}|\ldots|\Delta\boldsymbol{\xi}_{\boldsymbol{k,1}}\right]\right) \leq n_\xi - 1$ then $\dim(Ker\ \Xi) \geq 1$ and there exists $\boldsymbol{\vartheta_k} \neq 0$ such that ${\Delta\boldsymbol{\xi}_{\boldsymbol{k,i}}}^T\boldsymbol{\vartheta_k} = 0,\ \forall i = 1,\ldots,n-1$ and, hence, the vector $\boldsymbol{m_k} = \binom{0}{\boldsymbol{\vartheta_k}} \in \mathbb{R}^n \setminus \{0\}$ is orthogonal to $\bar{\boldsymbol{s}}_{\boldsymbol{k,n-1}},\ldots,\bar{\boldsymbol{s}}_{\boldsymbol{k,1}}$, which yields $\boldsymbol{m_k} = \alpha\boldsymbol{\pi_k}$ for some $\alpha \neq 0$. We deduce that $\boldsymbol{w_k} = 0$.

Remark. From Theorem 1 and Proposition 1, we deduce that if $\dim\left(Im\left[\Delta\boldsymbol{\xi}_{\boldsymbol{k,n}}|\ldots|\Delta\boldsymbol{\xi}_{\boldsymbol{k,1}}\right]\right) = n_\xi$ *then* $\boldsymbol{w_k} \neq 0$ *and, for every* $\Delta\boldsymbol{\xi}_{\boldsymbol{k+1,1}} \in \mathbb{R}^{n_\xi}$ *, we can choose* $\Delta\boldsymbol{u}_{\boldsymbol{k+1,1}} \in \mathbb{R}^{n_u}$ *for obtaining a vector linearly independent* $\bar{\boldsymbol{s}}_{\boldsymbol{k+1,1}}$ *with respect to* $\bar{\boldsymbol{s}}_{\boldsymbol{k,1}},\ldots,\bar{\boldsymbol{s}}_{\boldsymbol{k,n-1}}$*. Otherwise, if* $\dim\left(Im\left[\Delta\boldsymbol{\xi}_{\boldsymbol{k,n}}|\ldots|\Delta\boldsymbol{\xi}_{\boldsymbol{k,1}}\right]\right) < n_\xi$ *and* $\Delta\boldsymbol{\xi}_{\boldsymbol{k+1,1}}$ *is not generated by previous data, we assume that, for every* $\Delta\boldsymbol{u}_{\boldsymbol{k+1,1}} \in \mathbb{R}^{n_u}$, $\bar{\boldsymbol{s}}_{\boldsymbol{k+1,1}}$ *is linearly independent with respect to* $\bar{\boldsymbol{s}}_{\boldsymbol{k,1}}, \bar{\boldsymbol{s}}_{\boldsymbol{k,1}},\ldots,\bar{\boldsymbol{s}}_{\boldsymbol{k,n-1}}$*. Indeed, let* $\alpha_1,\ldots,\alpha_{n-1}$ *be constants in* $\mathbb{R}$ *such that* $\alpha\bar{\boldsymbol{s}}_{\boldsymbol{k+1,1}} + \sum_{i=1}^{n-1}\alpha_i\bar{\boldsymbol{s}}_{\boldsymbol{k,i}} = 0$*. Then, we have* $\alpha\Delta\boldsymbol{\xi}_{\boldsymbol{k+1,1}} + \sum_{i=1}^{n-1}\alpha_i\Delta\boldsymbol{\xi}_{\boldsymbol{k+1,i}} = 0$ *and* $\alpha\Delta\boldsymbol{u}_{\boldsymbol{k+1,1}} + \sum_{i=1}^{n-1}\alpha_i\Delta\boldsymbol{u}_{\boldsymbol{k+1,i}} = 0$*, and since* $\Delta\boldsymbol{\xi}_{\boldsymbol{k+1}}$ *is not generated by previous data, we deduce that* $\alpha = 0$*. Hence,* $\sum_{i=1}^{n-1}\alpha_i\bar{\boldsymbol{s}}_{\boldsymbol{k,i}} = 0$ *and it follows from the linear independence of* $\bar{\boldsymbol{s}}_{\boldsymbol{k,1}},\ldots,\bar{\boldsymbol{s}}_{\boldsymbol{k,n-1}}$ *that* $\alpha_1 = \cdots = \alpha_{n-1} = 0$.

Therefore, the difficult case is when $dim\left(Im\left[\Delta\boldsymbol{\xi}_{\boldsymbol{k,n}}|\ldots|\Delta\boldsymbol{\xi}_{\boldsymbol{k,1}}\right]\right) < n_\xi$ *and* $\Delta\boldsymbol{\xi}_{\boldsymbol{k+1,1}}$ *is a linear combination of* $\Delta\boldsymbol{\xi}_{\boldsymbol{k,1}},\ldots,\Delta\boldsymbol{\xi}_{\boldsymbol{k,n-1}}$*. If* $\Delta\boldsymbol{\xi}_{\boldsymbol{k+1,1}}$ *is a random vector, this event has null probability. Nevertheless, if this improbable case happens, then it is necessary to wait for new values of* $\boldsymbol{\xi}$*. In practice, components of* $\Delta\boldsymbol{\xi}_{\boldsymbol{k,1}},\ldots,\Delta\boldsymbol{\xi}_{\boldsymbol{k,n-1}},\Delta\boldsymbol{\xi}_{\boldsymbol{k+1,1}}$ *may remain unaltered. Under this scenario, we can reduce the dimensions of the uncontrolled variable, in order to estimate a reduced gradient in the space of the disturbances.*

4. Application to flotation column

The proposed methodology has been applied to an experimental setup that emulates a flotation column for copper concentration since it represents a relevant field of application for the Chilean production sector. Additionally, it fulfills the requirements of estimating the most important disturbances on a regular basis.

4.1 Description of the system

Copper is found in nature as oxides or sulfides. Copper sulfides represent the species with more abundance in Chile. For extracting the copper from primary sulfides (such as chalcopyrite), the ore extracted from the mine must be comminuted from 20 inches to 75 microns. After this stage, a liquid-solid mixture is concentrated from 0.5% to approximately 30% in weight using flotation. The industrial flotation process has three main interconnected zones: rougher, scavenger and cleaner, plus a regrinding stage. Figure 4 shows a typical flotation circuit. Each zone has specific equipment to fulfill their principal purposes. In particular, we are interested in the cleaning zone of the flotation circuit, where columns are used because of their capability to increase the concentration of the product, because of the use of washing water, among other factors.

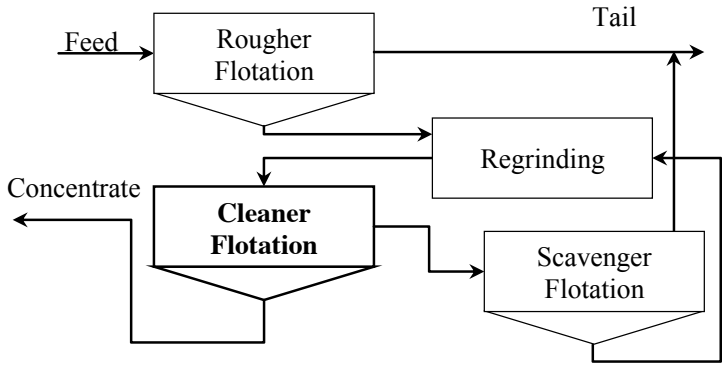

Figure 4. Flotation circuit scheme.

Figure 5 shows a diagram of a flotation column. It consists of a system with three inflows: feed pulp, air and wash water; and two outflows: concentrate and tail. Feed pulp with the valuable mineral comes from rougher cells and enters in the middle section of the column. Airflow is injected into the bottom to generate bubbles to collect the precious metal. Wash water is introduced at the top of the column by countercurrent with respect to air, with the aim to decrease the gangue of the concentrate. Concerning the outflows, the concentrate rich in the valuable mineral is collected at the top of the column; on the other hand, the tail flow leaves the column from the bottom and is sent to the scavenger concentration units to recover part of the remaining floatable minerals.

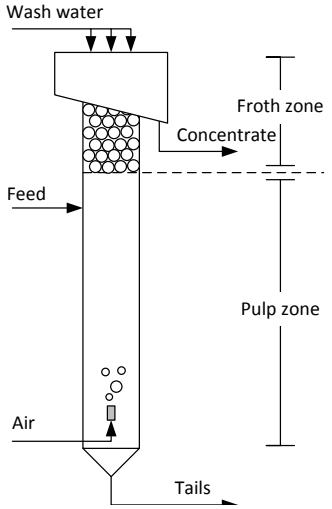

Figure 5. Flotation column diagram.

The column consists of two distinct zones: the collection zone and the cleaning zone. In the former, particles from the feed pulp are countercurrent with a rising group of bubbles produced at the bottom of the column, through a sparger. Here is where hydrophobic particles, i.e., floatable particles, collide with air bubbles and are transported to the top of the column, which is the cleaning zone. In the cleaning zone, the froth is formed because of the addition of chemical reagents and wash water cleans the froth from gangue particles.

The properties of the feed pulp change because of the operation of side units and the quality of the raw materials. In particular, variables that affect the mass transfer are continuously monitored or estimated, such as the concentration of copper (grade of feed), solid percentage and particle size. Therefore, data of disturbances are available to be included in a supervisory layer based on real-time optimization. Moreover, the flotation column presents two manipulated variables to modify the metallurgical objectives of the process: froth depth and air hold-up.

The metallurgical objectives of the process are known as recovery and grade. Eq. (17) shows the expression to calculate the Recovery (R) as the percentage of copper of the feed that is recovered at the concentrate, while the grade of copper corresponds to its concentration. A trade-off exists between both objectives, since a higher grade of copper implies a lesser recovery because of the mechanical drag produced by the water in the cleaning zone.

$$R \coloneqq \frac{F_C \cdot C_C^{Cu}}{F_F \cdot C_F^{Cu}}, \quad L \coloneqq C_C^{Cu} \tag{17}$$

where F_C and F_F are the flows, and C_C^{Cu} and C_F^{Cu} are the copper concentrations in the concentrate and in the feed, respectively.

4.1.1 Input Variables

Controlled Variables

The variables usually controlled are bias, air hold-up and froth depth. In the laboratory-scale flotation column, bounds were implemented on exponential changes in the control loop for avoiding problems in the control performance. The maximum step changes for froth depth and hold-up control loops were between 25% and 40% of the span, respectively (see Table 1).

Table 1. Operational ranges for controlled variables.

Variable	Lower bound	Upper bound	Unit
$\boldsymbol{H_f}$	40	120	cm
$\boldsymbol{\epsilon_G}$	8.0	15.0	%
$\boldsymbol{B}$	0.0	0.80	L/min

- Gas hold-up (ϵ_G): it is defined as the fraction of air inside the column. Air hold-up is an important variable because it can affect considerably the particle residence time and mineral collection, and it depends on air rate, bubble diameter, pulp density and concentration of chemical reagents, among other variables (Yianatos et al., 1986).

  For an air-water system with constant density, this variable can be estimated as shown in Eq. (18).

$$\epsilon_G \coloneqq 1 - \frac{\Delta P}{\Delta L} \tag{18}$$

where ΔP is the pressure difference in the collection zone in [$\mathrm{cmH_2O}$]. ΔL is the distance between the pressure sensors in [cm].

- Froth depth (H_f): it corresponds to the height of the froth measured from the froth-pulp interface to the top of the froth, and it was measured in [cm].

- Bias (B): it is defined as the net downward flow of water crossing the froth-pulp interface, it is calculated in stationary state as the difference between tail Q_T and feed Q_F flows (Eq. 19). Nevertheless, it was not considered in the supervision layer because controlling it in the flotation column has been problematic. It was measured in [L/min].

$$B \coloneqq Q_T - Q_F \tag{19}$$

Disturbances

As mentioned above, there is a flow of pulp entering the flotation column and coming from the re-grinding unit. The characteristics of this feed pulp are given by previous processes; therefore, for this work they were considered as disturbances. The variables considered correspond to the concentration of copper (x_F), the percentage of solids (S_F) and the particle size (D_{P_F}).

As shown by actual plant data, these variables change as a function of time due to the different characteristics of the mineral entering the concentrator. Depending on these features, the rougher stage configures its operational points, because it is the first one. Consequently, all downstream units are operated according to those mineral conditions. Additionally, it is known that the conditions and characteristics of ore entering the concentrator change, because the material contained in the piles after grinding is used, and in these, the material has no uniform characteristics.

4.1.2 Output variables

The output variables correspond to the variables measured in the operation of the floatation column. These can be obtained with instrumentation as shown in Figure 6 and correspond to flow measurements, pulp-foam interface position and concentration.

The primary objectives, as indicators of process productivity and product quality, are recovery and concentrate law. Since the direct estimation of these variables requires intensive maintenance and calibration of the on-line analyzers, secondary objectives are controlled in the flotation column, such as froth depth, gas flow rate and wash water flow rate (Bergh & Yianatos, 1993). In this paper, the secondary objectives mentioned in Section 4.1.1 above are controlled.

4.1.3 Experimental setup

The supervisory layer was implemented in the laboratory-scale flotation column shown in Figure 6. The body of the column is an acrylic cylinder with an internal diameter of 9.2 cm and height of 3.27 m, with a system to collect the froth at the top by overflow. The experimental setup is a closed loop

for both water and frother (chemical reagent), as shown in Figure 3, and E-1 is a recirculation tank where these are contained.

The feed and the wash water are pumped using two peristaltic pumps. The air is injected from the compressed air line through a porous diffuser. Both the air and tail flows are manipulated using globe valves with pneumatic 3–15 psig actuators. The column has two pressure transmitters in the collection zone, a volumetric flowmeter for the tail, and a mass flowmeter for the air. Table 2 summarizes the instrumentation.

Table 2. Instrumentation of the flotation column.

Tag	Description	Type	Brand and model
PT-1	Pressure transmitter	Membrane	Delta controls – DAPC-2000/ALW
PT-2	Pressure transmitter	Membrane	Delta controls – DAPC-2000/ALW
FI-1	Tail flowmeter	Tangential turbine	Omega – FPR-204 PC
FI-2	Air flowmeter	Mass	Aalborg – GFM 37
P-1	Feed pump	Peristaltic	Masterflex–77411-00/77601-00 Head
P-2	Wash water pump	Peristaltic	Masterflex – 7528-10/77800-52 Head

Three control loops were implemented in the flotation column. These are presented in Figure 6, where the P&ID diagram is shown. The configuration follows the typical pairing for this type of unit: H_f – tail flow (LIC), ε_G – air flowmeter – air flow (DYC-FIC) and B – wash water flow. However, while the RTO layer was operating, the bias control loop was open due to the coupling problem between the H_f and bias control loops. The regulatory layer was implemented with PID controllers in a GE Fanuc 90-30 series PLC.

According to the control loops configured in the flotation column, the manipulated variables are the tail, air and wash water flows. These variables affect the flotation process in the column in the following ways:

- **Tail flow**: its performance allows increasing or decreasing the amount of froth present in the column. This relates to the residence time of both zones within the column. An increase in this variable causes a decrease in the volume of the collection area, decreasing residence time, decreasing recovery and increasing the grade.
- **Airflow**: its action allows manipulating the airflow entering the column. Consequently, a higher flow increases the concentration of gas contained in the column, then more valuable mineral is recovered. Nevertheless, the grade of valuable mineral is diminished, due to the increased probability of collisions between air and particles.
- **Wash water:** if the bias control is active, this variable can be manipulated to increase the entrainment of the gangue particles that are floated, which increases the cleaning and thus the grade also rises; however, a decrease occurs in recovery.

The implementation in the laboratory-scale flotation column was made using a hybrid approach, as the presented by Bergh (2007, 2012) and Bergh & Yianatos (2011, 2014). This means that essential phenomena can be divided into two aspects: hydrodynamics and physicochemical mechanisms.

The hydrodynamics of flotation process can be represented using an air-water system, whereas the physicochemical mechanism was represented by a metallurgical simulator of flotation copper sulfide minerals that uses a first-principles model with two types of degrees of freedom: physical and virtual. The physical degrees of freedom are the variables measured from the experimental air-water setup and the design parameters of the column. The virtual degrees are emulated characteristics of feed pulp, i.e., mineralogical composition, physical properties of mineralogical species, solid percentage, grade and particle size, together with the kinetic relations that allow us to calculate the recovery and grade of the concentrate (Bergh, 2007, 2012). This approach has been proven to be a good alternative for the study of supervisory mechanisms in metallurgical processes (Bergh & Yianatos, 2011).

As mentioned by Navia et al. (2016), the dynamic of the experimental setup is controlled by the actuator of froth depth control loop, i.e., the tail valve. The tail flow is produced due to pulp level, so its dynamics is on the order of minutes. Gas enters at the bottom, and it is discharged to the atmosphere at the top of the column, whose dynamic is on the order of seconds. Then, the dominant dynamic of the column is related to H_f and the tail flow, and the interaction between froth depth and bias control loops.

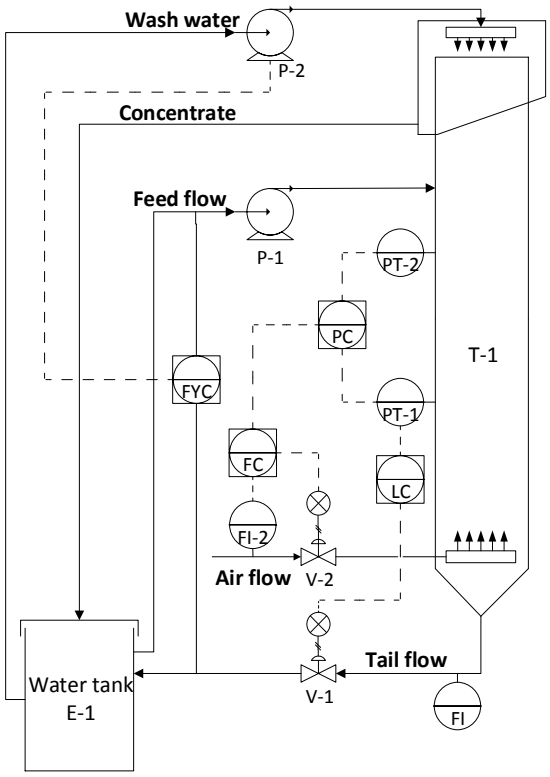

Figure 6. P&ID of the flotation column.

4.1.4 Metallurgical model

A combination of phenomenological and empirical models of the flotation process was used to represent a three-phase system with variable input conditions, due to its high complexity. This model is based on the analysis proposed by Finch & Dobby (1990).

In a flotation column, the concentration process can be calculated by considering a different model for each zone of the equipment. Thus, exponential functions are used to calculate the recovery in the cleaning (R_f) and collection (R_C) zones (Yianatos et al., 1998; Yianatos et al., 2005).

$$R_{f,i} = P_{R_f,i} \cdot exp\left(\frac{-0.0144 \cdot H_f \cdot (1+3 \cdot J_w)}{J_G^3}\right)$$

$$R_{C,i} = P_{R_C,i} \cdot \left(1 - \frac{4}{3 \cdot K_{C,i} \cdot \tau_C} \cdot \left(\frac{10}{9} \cdot ln\left(\frac{10 \cdot K_{C,i} \cdot \tau_C + 12}{K_{C,i} \cdot \tau_C + 12}\right) - 1 + \frac{12}{K_{C,i} \cdot \tau_C + 1}\right)\right) \quad (20)$$

$$\tau_C = \frac{V_C \cdot (1-\epsilon_G)}{Q_F}$$

The parameters in Eq. (20) were adjusted considering two mineralogical species i: chalcopyrite and gangue, where $R_{f,i}$ and $R_{C,i}$ represent recovery in the cleaning and collection zones, respectively; H_f is the froth depth; J_G and J_W are the surface velocities of the gas and the wash water, respectively; τ_c corresponds to the residence time of the solid in the collection zone, where V_c is the volume of the collection zone, ε_G is the gas concentration, and Q_F is the volumetric feed flow.

In Eq. (20), $K_{C,i}$ represents the kinetic floatability constant of species i and is related to the probability of collision of the gas with the mineral particles. On the other hand, Eq. (21) shows $K_{C,i}$ as function as gas surface velocity J_G and particle diameter D_p, where the parameters were obtained from data collected in the column, setting operating points equivalent to maximum recovery on the one side, and maximum concentration on the other.

The kinetic constant in the collection zone for species i is (Bergh et al., 1998):

$$K_{C,i} = k_{c,i} \cdot J_G^{0.75} \cdot \left(A + B \cdot D_p + C \cdot D_p^2\right) \quad (21)$$

4.2 Implementation of the RTO layer

The implementation of the RTO layer is shown schematically in Figure 7, where the output of the optimization stage corresponds to the set point values of the froth depth control loops (H_f) and the hold up (ϵ_G). The optimization variables are defined as $u^T \coloneqq [H_f, \epsilon_G]$. After the application of these set points, the system must reach a steady-state, which is verified through a statistical model proposed by Rhinehart (1995), and it is based on using the variance of the controlled variables.

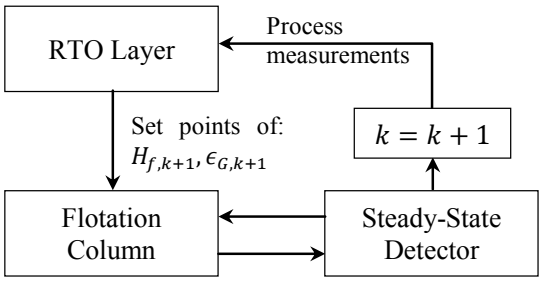

Figure 7. Implementation diagram of the RTO layer.

4.2.1 ARIMA for modeling disturbances

In general, there is a limitation to the availability of the data measured by the control systems, since these are often delayed and sometimes require pre-processing to be available for other layers of operation (e.g., optimization). Particularly in the processing of minerals, it becomes more complex to have measurements of some variables of interest, for example, the measures of grade require chemical analysis in the laboratory to be able to count on this data, and so at the instant known that measurement the mineral has already been processed.

With this in mind, and as mentioned previously, it is proposed to use an ARIMA (Auto Regressive Integrated Moving Average) model to estimate values of variables that are difficult to quantify online. The main reason is that a large amount of historical data of operation gives an idea of the future changes in the variables that have a high level of autocorrelation.

According to the methodology presented by Box et al. (2015) in Chapter 4, the models corresponding to each disturbance were obtained: feed grade, solids percentage and particle diameter are as shown in Eq. (22); these variables are represented by z_t, and the variable a_t corresponds to the stochastic part of the model.

$$\phi_p(B)\Phi_P(B^s)\nabla^d\nabla_s^D z_t = \theta_q(B)\Theta_Q(B^s)a_t \tag{22}$$

Where p corresponds to the order of the autoregressive part of the model, d is the order of differentiation of the non-seasonal part, q is the order of the moving average, P is the order of the seasonal autoregressive part, D is the order of differentiation of the seasonal part, Q is the order of the seasonal moving average part, s is the period of the time series, B represents the backward shift operator, and ∇ is the backward difference operator.

4.2.2 Objective Function

The objective function is the inverse of the economic benefit of the flotation column in (USD/h). Navia et al. (2016) presented an objective function that does not consider some operational costs of side units. Therefore, they are included in this work. The function is shown in Eq. (23):

$$P = (Incomes - Costs_{Op}) \tag{23}$$

The incomes correspond to the gain obtained from the sale of copper concentrate, whose value depends on the grade of concentration and the price per pound of copper according to the London Metal Exchange. These are calculated according to Eq. (24), where C represents the flow of concentrate of dry mineral, which is calculated by mass balance, and P_{conc} is the price of the concentrate.

$$Incomes = C \cdot P_{conc} \tag{24}$$

On the other hand, the operational costs ($Costs_{op}$) shown in Eq. (25) were divided into energy costs, due to reprocessing the recycled material to adjacent units, and losses of valuable mineral exiting as tail flow in the scavenger circuit.

Furthermore, energy costs ($Costs_E$) correspond to those required to pump the water and inject air into the column, as shown in Eq. (25). Those costs were estimated according to the price of the energy and considering the specific energy of pumping (C_P) and compression (C_c) of the experimental system.

Additionally, mineral loss costs ($Costs_{loss}$) corresponds to the mineral that is recovered in the cleaner stage and cannot be recovered in the scavenger circuit, which has a high recovery (R_{SC}), approximately 97%, according to experimental data, see Eq. (25).

Moreover, reprocessing costs ($Costs_R$) represents the reprocessing of the mineral that is recycled in the subsequent stage. This includes the costs of re-grinding per ton of dry mineral (C_{RG}) equal to 5.75 $\frac{USD}{MWh}$ (Ipinza, 2009), and the marginal cost of electricity (C_E) in the "*Sistema Interconectado del Norte Grande (Chile)*" is 49 $\frac{USD}{MWh}$ (Coordinador Eléctrico Nacional, 2017) (see Eq. 25).

$$\begin{aligned} Costs_E &= P_E \cdot (Q_F C_{P,F} + Q_W C_{P,W} + Q_A C_C) \\ Costs_{loss} &= (1 - R_{sc}) \cdot (1 - R_{Cu}) \cdot x_F \cdot F \cdot P_{Cu} \\ Costs_R &= (1 - R_{sc}) \cdot T \cdot C_{RG} \cdot C_E \end{aligned} \tag{25}$$

4.2.3 Uncertainty in the model-based optimization

As mentioned in Navia et al. (2016), in this application, uncertainty in the model-based optimization originated from experimental and simulated sources. The simulated uncertainty has been implemented as a mismatch in the physicochemical description of $R_{C,i}$ for both species. Although flotation can be described as a pseudo-first-order reaction, the physical dependencies for recovery are still not fully understood (Savassi, 2005). In this work, this uncertainty has been simulated using the mismatch from Eq. (26) in the description of $K_{C,i}$ for the model implemented in the RTO.

$$K_{C,i} = \frac{\sum_j^{N_e} K_{C,i,j}(\boldsymbol{u}, \boldsymbol{\alpha})}{N_e}, \forall\, i = 1{,}2\ (chalcopyrite, gangue) \tag{26}$$

where $K_{C,i}$ is the kinetics constant for species i and was calculated as the mean of the N_e operational points performed for the operational variables model that depend on the optimization variables $\boldsymbol{u}$ and the fitted parameters $\boldsymbol{\alpha}$. A comparison between Eqs. (20) and (25) illustrates that the simulated uncertainty in $R_{C,i}$ can be classified as structural because the model neglects the influence of operational conditions in flotation kinetics.

On the other hand, the experimental uncertainty is related to the action of the regulatory layer and the precision of control instruments. However, another source of uncertainty in this work is the regression done to describe a relationship between operational variables and controlled variables. This was achieved through a linear model, which allows optimizing the metallurgic result as a function of the previously selected inputs variables: H_f, ϵ_G and B.

For describing a metallurgical simulator of a flotation column, it is necessary to relate the operational variables with the controlled variables (or degrees of freedom of the system), through an experimental design 2^3 and 4 central points. Therefore, three responses were measured, which are gas (J_G), wash water (J_w) and bias (J_b) surfaces velocities. With these results, the process can be evaluated economically by simulating the operation. Table 3 presents the complete details for the experimental design, where the minimum and maximum values for hold up (ϵ_G) were [8%; 15%], for the froth height (H_f) were [40 cm; 120 cm], and for bias (B) were [0 L/min; 1 L/min].

Table 3. Experimental design for describing a metallurgic simulator.

Nº exp	ϵ_G [%]	H_f [cm]	B [L/min]
1	8.0	40	0.0
2	15.0	40	0.0
3	8.0	120	0.0
4	15.0	120	0.0
5	8.0	40	1.0
6	15.0	40	1.0
7	8.0	120	1.0
8	15.0	120	1.0
9	11.5	80	0.5
10	11.5	80	0.5
11	11.5	80	0.5
12	11.5	80	0.5

According to the experimental design, models such as Eq. (27) are proposed for the three responses, where x_1 corresponds to froth height, x_2 to hold up and x_3 to bias. The parameters obtained for the model of surface velocities are shown in Table 4.

$$J_i = b_{0,i} + \sum_{l=1}^{3} b_{l,i} \cdot x_l + \sum_{l=1}^{3} \sum_{m<l} b_{lm,i} \cdot x_l \cdot x_m + b_{123,i} \cdot x_1 \cdot x_2 \cdot x_3, \qquad \forall i \in \{G, w, B\} \tag{27}$$

Table 4. Parameters of the model of surface velocities.

Parameter	J_G	J_w	J_b
b_0	1.30e-01	3.364e-2	3.41e-04
b_1	-1.91e-03	0	-4.19e-06
b_2	2.26e+01	0	0
b_{12}	-8.00e-02	0	0
b_3	0	2.249e-1	2.51e-01
b_{13}	0	0	1.58e-06
b_{23}	0	0	0
b_{123}	0	0	0

It was determined that the surface velocity of wash water does not depend on the decision variables; instead, it depends on the controlled variable bias whose variation along the experimental run served to determine the parameters of the model; therefore, it is expected that this variable depends significantly more on the bias than on the decision variables, since the wash water corresponds to the control loop actuator of that degree of freedom.

4.2.3 Model-based optimization

The constraints imposed on the studied problem were given by the operational limits of some process variables, specifically, the superficial velocities of gas, wash water and bias. Additionally, limits were established for metallurgical performance variables and the grade of copper in the concentrate. All of these variables, which are shown in Table 5, are affected by structural uncertainty.

Table 5. Constraints of the optimization.

Variable	Lower bound	Upper bound	Units
J_G	1.0	2.0	cm/s
J_w	0.04	0.4	cm/s
J_B	0.0	0.28	cm/s
R_{Cu}	55	100	%
x_C	22	34	%w/w

On the other hand, to identify the point at which the system was to converge, both for offline and online implementation, the optimization was solved using the complete phenomenological model, i.e., without structural uncertainty. This point was identified as the optimum of the process. Similarly, the optimization result used in the uncertain model constructed according to Eq. (26) was defined as optimal for the model. The values of the kinetics constants were calculated using the experimental run shown in Table 1, where the average of all preliminary points represents $K_{C,i}$ for the uncertain model.

The optimization problem is explained in Eq. (28), where the objective function and the constraints depend on the decision variables $\boldsymbol{u}$ and the parameters of the model $\boldsymbol{\alpha}$. This optimization problem also includes the modifier of the objective function: $\boldsymbol{\lambda_k}$, and the modifiers $\boldsymbol{\gamma_k}$ and $\boldsymbol{\varepsilon_k}$ of the constraints.

$$\begin{aligned} &\min_{u\in U} -P_m(\boldsymbol{u},\boldsymbol{\alpha}) + \boldsymbol{\lambda_k^T u} \\ &s.t.: \\ &\boldsymbol{C_m}(\boldsymbol{u},\boldsymbol{\alpha}) + \boldsymbol{\gamma_k^T}(\boldsymbol{u}-\boldsymbol{u_k}) + \boldsymbol{\varepsilon_k} \leq 0 \\ &|(\boldsymbol{u}-\boldsymbol{u_k})^T \boldsymbol{w_k} + (\boldsymbol{\xi_{k+1}}-\boldsymbol{\xi_k})^T \boldsymbol{\vartheta_k}| \geq \delta \end{aligned} \tag{28}$$

Please note that dual constraint depends on the disturbances of the process $\boldsymbol{\xi_k}$. In Eq. (28), $\boldsymbol{u}$, $\boldsymbol{\xi}$, and $\boldsymbol{C_m}$, are defined as Eq. (29), being superscripts UB and LB upper and lower bounds of the given variable, respectively.

$$\boldsymbol{u} = \begin{bmatrix} H_f \\ \epsilon_G \end{bmatrix}, \qquad \boldsymbol{\xi} = \begin{bmatrix} x_F \\ S_F \\ D_{P_F} \end{bmatrix}, \qquad \boldsymbol{C_m} = \begin{bmatrix} J_G - J_G^{UB} \\ J_G^{LB} - J_G \\ J_w - J_w^{UB} \\ J_w^{LB} - J_w \\ J_B - J_B^{UB} \\ J_B^{LB} - J_B \\ R_{Cu} - R_{Cu}^{UB} \\ R_{Cu}^{LB} - R_{Cu} \\ x_C - x_C^{UB} \\ x_C^{LB} - x_C \end{bmatrix} \tag{29}$$

As mentioned previously, the modifiers depend on the process gradients, for this work the directional derivative approach was used for all cases. The main feature of this method is that it allows the use of previous states for the estimation of gradients by summing an additional constraint to the system, related to the degree of excitation necessary to estimate the gradients (Brdys & Tatjewski, 1994).

5. Results

In this chapter, we present the results obtained from simulation and experimentation. It shows the evolution of the decision variables and the objective function.

In each graph, the optimum of the model ($\boldsymbol{u_m^*}$) is presented as a red dashed line, the optimum of the process ($\boldsymbol{u_p^*}$) is the blue dash-dot line and the operating value of the variable ($\boldsymbol{u_k}$) is the solid black line. In addition, the limits of the decision variables are the dashed gray lines ($\boldsymbol{u^L}, \boldsymbol{u^U}$), and the disturbances ($\boldsymbol{\xi_k}$) are the solid black lines.

5.1 Simulation results

For the simulation of the process, it is assumed that the input variables change between each steady state, therefore changes in output variables are consequences of decision variables and disturbances.

First, the results obtained in the simulation are presented without the implementation of the proposed method, using an approximation of directional derivatives in the process gradient estimation. It is possible to appreciate the effect of the changes in the input conditions on the optimum of the system, which hinders the optimization layer from bringing the operation of the plant to the optimum point.

Second, the results obtained in the simulation show the application of the proposed method for the process gradient estimation, including the effect of the input variables. Therefore, the optimum of the plant was reached due to the correction in the gradient estimation step in the optimization layer.

Figure 8 shows the changes of the disturbances during the application of the optimization layer. The values of these variables are assumed to be consequences of processes before the cleaner stage. These data were simulated through an ARIMA model that had been previously obtained by using real data of variables measured in the operation of a flotation column.

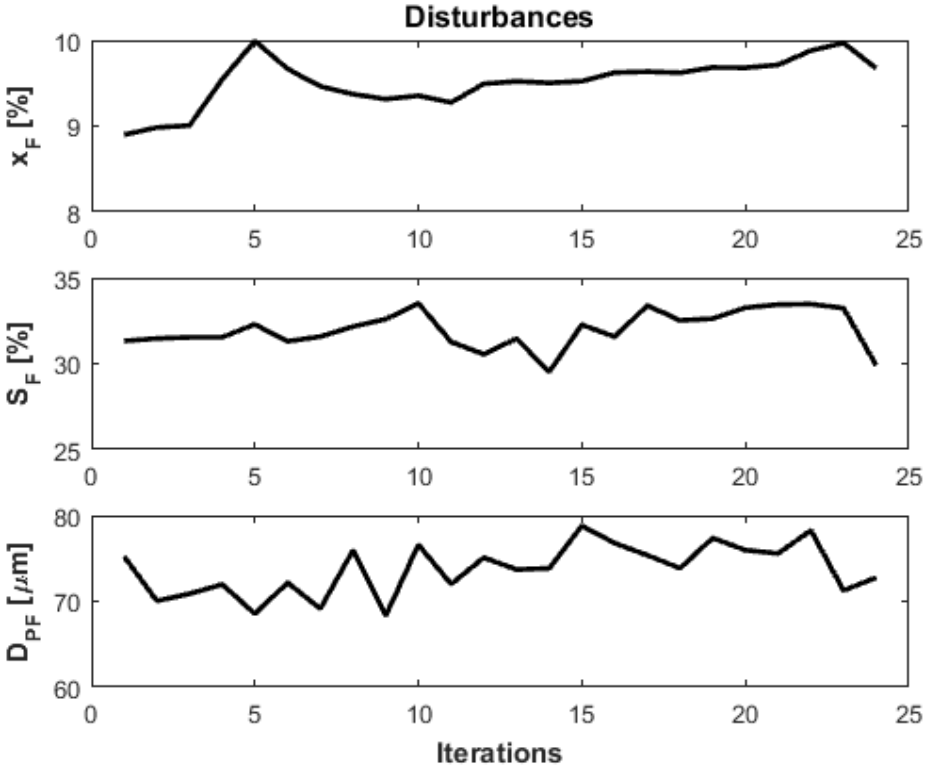

Figure 8. Inputs variables versus iteration number.

5.1.1 Gradients of the process without correction

Figure 9 shows the evolution of the economic benefit as function of iteration number. In this case, the gradient estimation step does not consider the changes in the input variables. The value of the objective function evolves in a similar form to the optimum of the process and model. However, the economic benefit obtained is 26% lower than the expected value.

On the other hand, according to Figure 10, the decision variables do not achieve convergence toward the optimum of the plant. It means that an erroneous process gradient estimation keeps the system from reaching the optimum. Therefore, it is proposed to make a gradient estimation that includes the changes in the disturbances, as shown in Section 5.1.2.

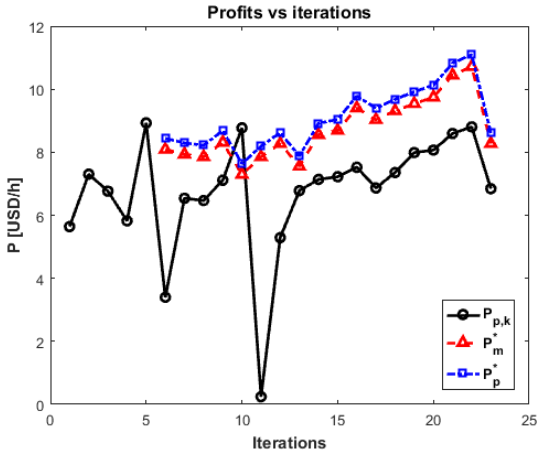

Figure 9. Profits in simulation without corrections in process gradients.

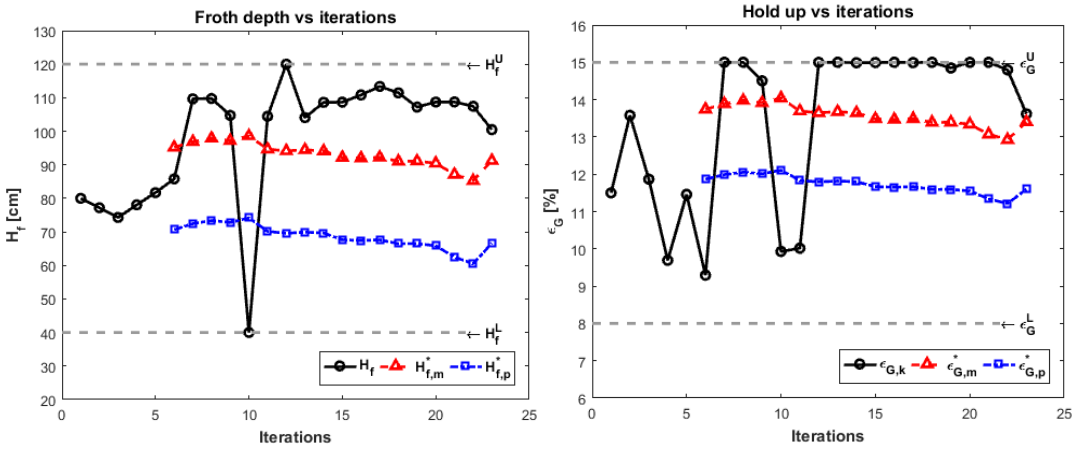

Figure 10. Decision variables in simulation without corrections in process gradients.

5.1.2 Gradients of the process with correction

Figure 11 shows the evolution of the economic benefit and how it increases as the optimization layer iterations rise, reaching up to 10.87 [USD/h] compared to the model values (10.80 USD/h) and the process (11.18 USD/h) cannot make a significant difference. The implementation is shown up to iteration 24, where 19 of these iterations correspond to resolutions of the optimization problem and the first six initial states ($n_u + n_\xi + 1$) for the estimation of gradients by the proposed method.

Figure 12 shows the evolution of the decision variables and its convergence towards the gray line, which represents the optimum of the process. In the simulation, this indicates that an appropriate estimation of gradients allows obtaining a real optimum operation.

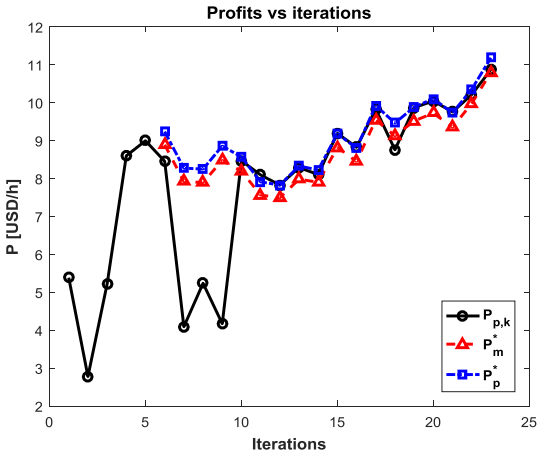

Figure 11. Profits in simulation with corrections in process gradients.

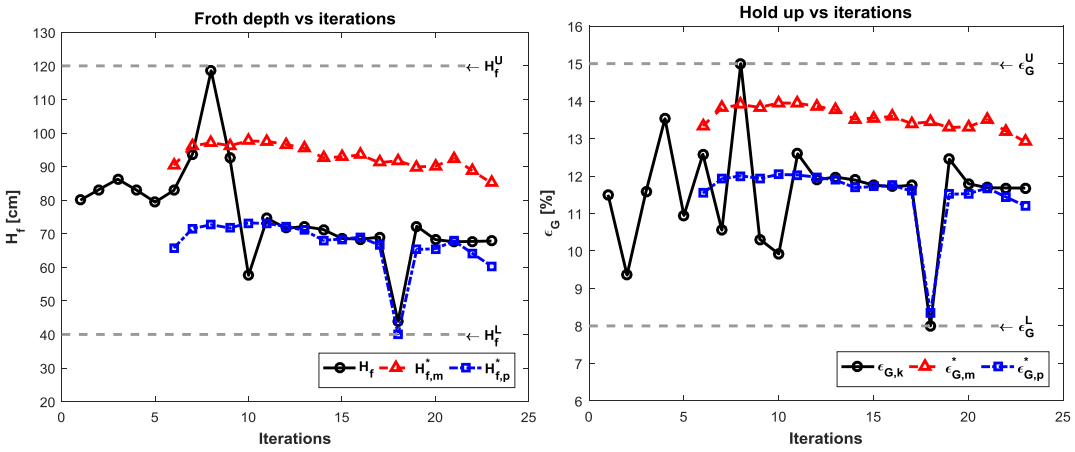

Figure 12. Decision variables in simulation with corrections in process gradients, using the proposed method.

5.2 Experimental results

Two different cases were performed in the experimental set-up. The first one assumes that there is an immediate knowledge of the input conditions, defined as the ideal case; in the second situation it is considered that the measurement of the input conditions is not available instantaneously, and only an estimate given by an ARIMA model is available, defined as a realistic case.

The initial operating point for both cases was 75 [cm] and 9 [%] for H_f and ϵ_G, respectively.

The implementation time is different because the first one evaluated the ability of the system to remain in an optimum condition, and if it escapes, it subsequently converges to the operational optimum; meanwhile, for the second it was expected that the system would reach optimum.

5.2.1 Ideal case

Figure 13 shows the simulated input conditions in this implementation. The results obtained show a long application of the optimization layer up to approximately 200 minutes. In addition, as shown in Figure 14 and Figure 15, it is possible to achieve an optimal operation of the flotation column at iteration six, and then at iteration 23, it diverges from the optimal condition for eight iterations (approximately) before converging again to the operation optimum of the process. The profit in the final part of the flotation column operation was approximately 6.5 [USD / h].

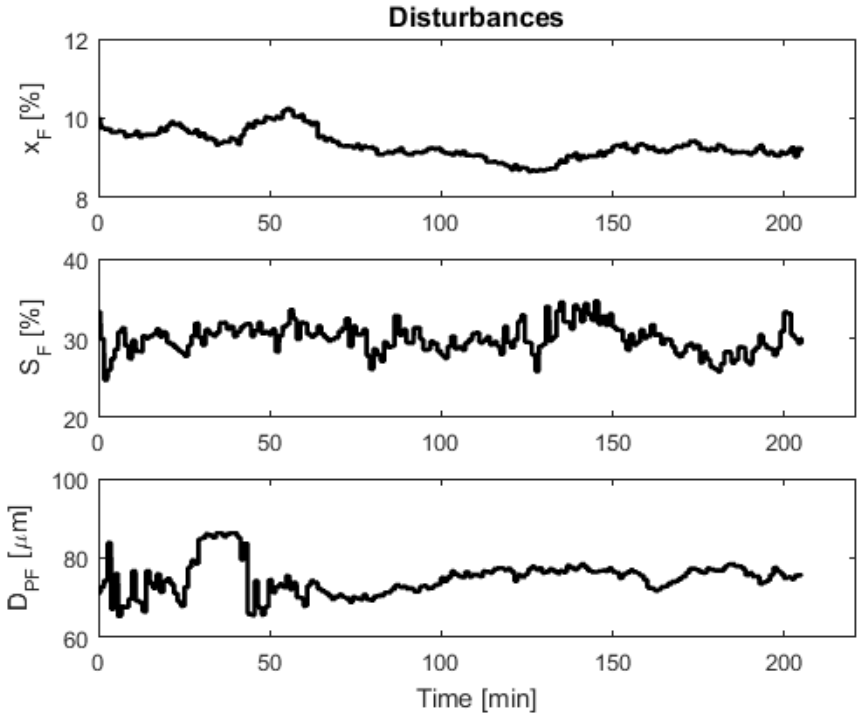

Figure 13. Inputs conditions versus time in the operation of the flotation column.

Figure 14 shows the evolution of profit during the implementation of the optimization layer, and it also shows the optimum of the process and model. A rise from the initial point of operation can be

noticed, reaching a value close to 7 [USD/h] in the last iteration. Moreover, from iteration 11, the system converges to the vicinity of the optimal operation, and it is maintained around the blue and red lines representing the optima of the process and model, respectively.

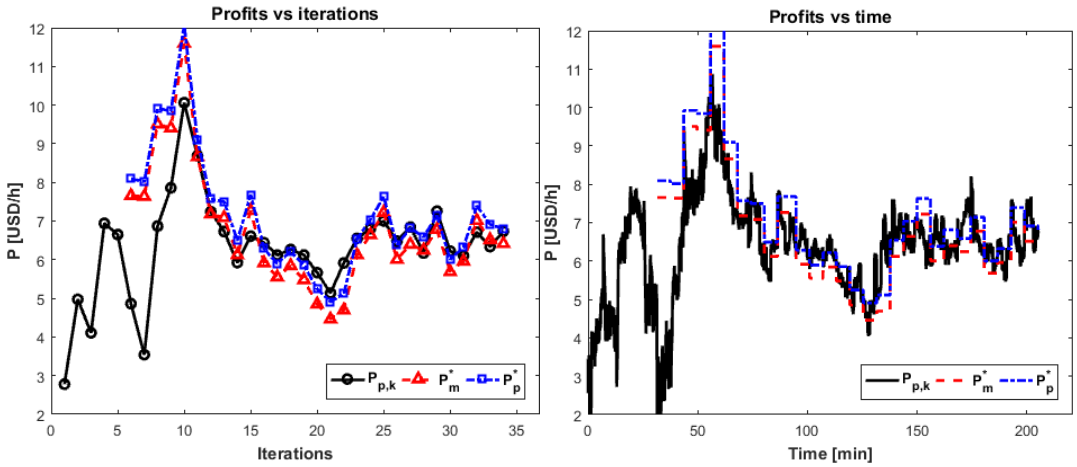

Figure 14. Profit versus iteration number in the RTO and time in the operation of the flotation column in the ideal case.

Figure 15 shows the evolution of the decision variables in the operation of the flotation column. The convergence toward the optimum of the process is achieved in iteration 15 approximately. Subsequently, at iteration 23, the system is decoupled from the optimum operation. Because of this change, it is possible to notice that the system takes approximately eight iterations to converge again to the operational optimum.

The decoupling mentioned above can be explained by the lack of identifiability in the system in iteration 23, according to Figure 15. Before this instant, the system did not have noticeable changes to be able to estimate the gradient in an appropriate form. Although the dual constraint is imposed, which ensures a minimum of system excitation, there is a trade-off between how much the system is forced to achieve identifiability and its stability.

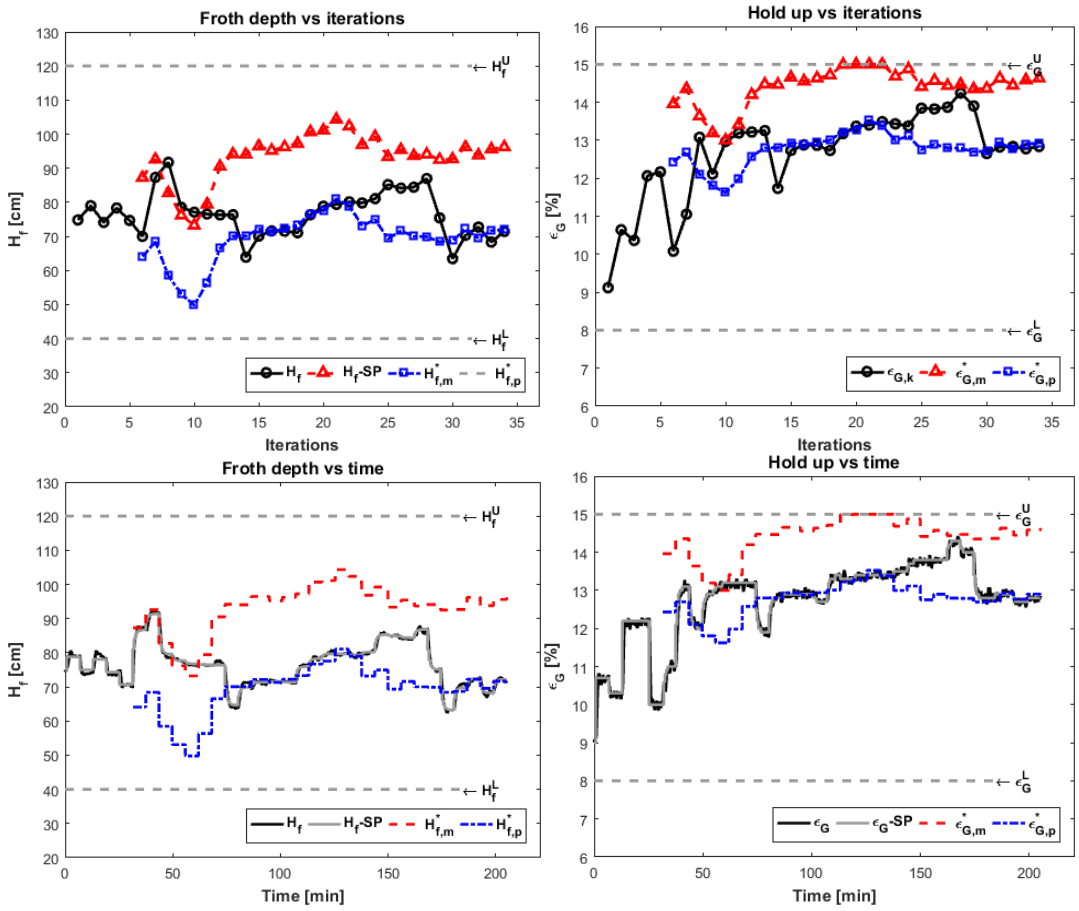

Figure 15. Decision variables versus iteration number and time for the ideal case.

5.2.2 Realistic case

The RTO layer was implemented with measurements of input conditions estimated by using ARIMA models. The purpose was to simulate a realistic situation, where the availability of some variables is not immediate since they are measurements obtained by laboratory analysis or another method that is not available online. The running time was 85 minutes.

The optimization problem was solved seven times to reach the operational optimum, as is shown in Figure 16. The profit increased with the implementation of the optimization layer, reaching a value equal to 6 [USD/h], close to the optimum of both process and model. With regard to the objective function, it is difficult to establish that the system converged toward the real optimum of the flotation column since there are no significant differences between the optimum values of the model and those of the process. However, according to Figure 17, the decision variables manage to reach the optimum of the process approximately at iteration number 15. At the last operational point shown, the froth depth differs by 8.42% from the expected value, while hold-up differs by 2.21%. Therefore, the system managed to reach the optimum operation of the laboratory-scale flotation column assuming a case with input variables estimated through an ARIMA model.

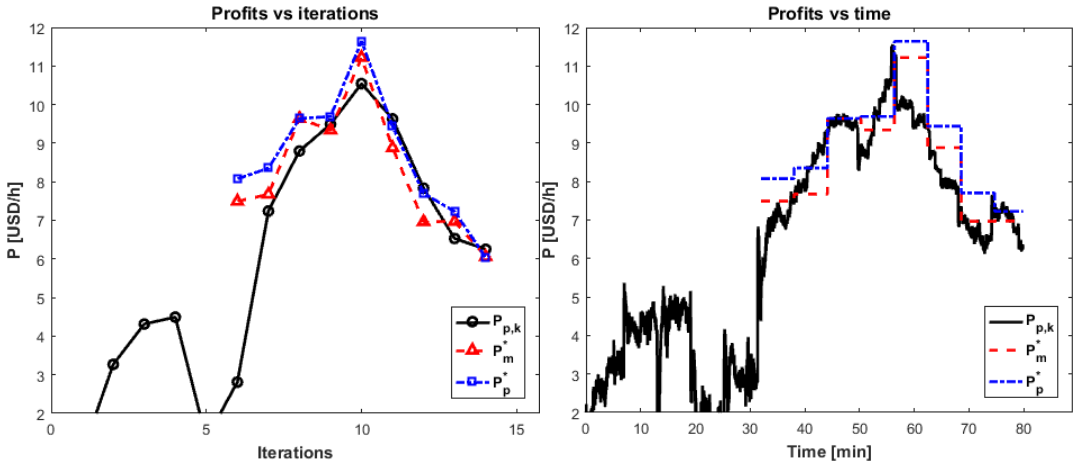

Figure 16. Profits versus iteration number and time for the realistic case.

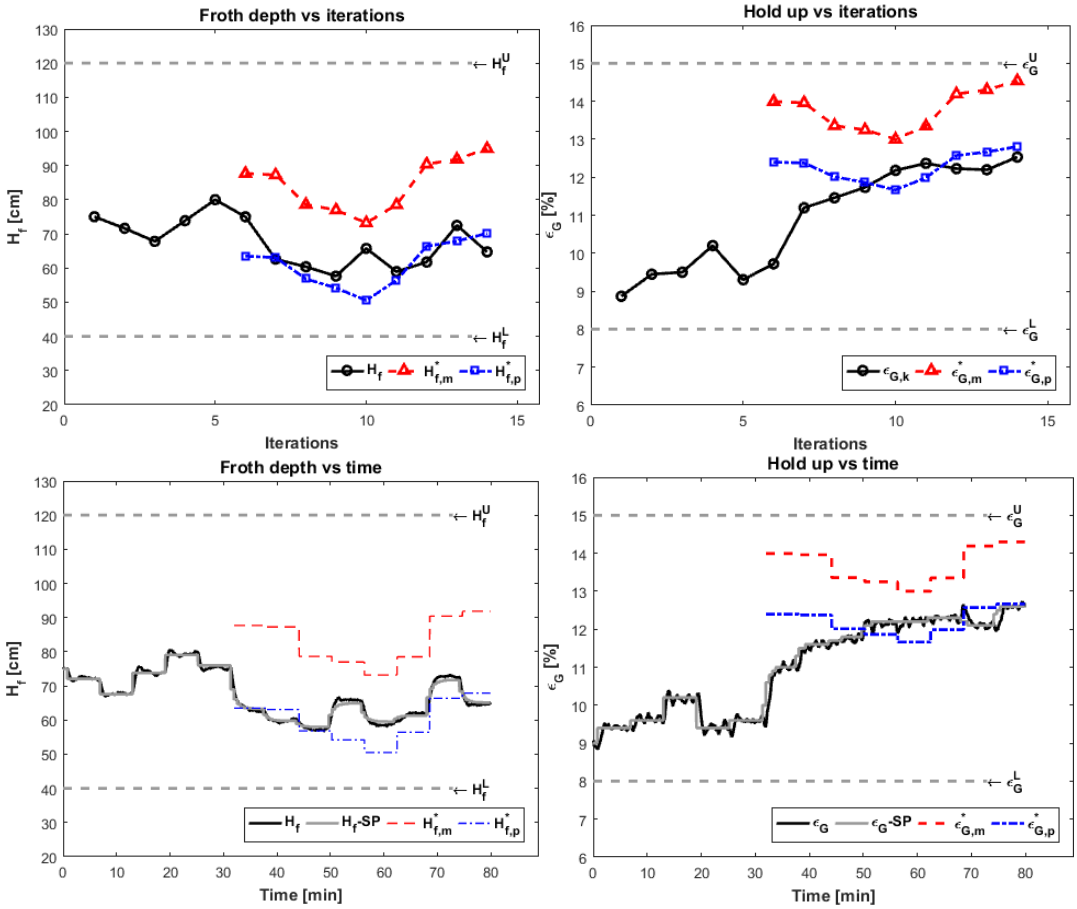

Figure 17. Decision variables versus iteration number and time for the realistic case.

6. Conclusions

In this work, an extended form of gradient estimation has been proposed in the MA method presented by Marchetti et al. (2010), in the RTO. The idea is to include the available information of significant disturbances, in order to create a more realistic scenario. This proposal was tested in simulations and in experiments.

Because the mining industry is one of the most important economic sectors in Chile, and since flotation columns are used at the end of the circuit of the concentration stage, this paper presents an implementation of an RTO layer to a laboratory-scale flotation column that includes the effect of disturbances from adjacent units. The results show that the optimal operation of the system changes under time-varying input conditions. Therefore, if the gradient estimation step does not consider the disturbances, the system could not converge to the desired operational point. In other words, the use of this extended gradient estimation method allows the optimal operation to be tracked when the feed characteristics change while the RTO layer is working, and consequently, the economic benefit of this process can be increased by 26%.

The experimental results show that the system achieved the optimal operation. During the implementation, the system presented a divergence from the optimal performance because the gradients were poorly estimated; this explains why, for the dual constraint, the application of the supervisory layer was made by prioritizing the stability of the system over identifiability. Additionally, two situations were analyzed: the ideal case, where the availability of disturbances data was immediately available; and the realistic case, where an ARIMA model gives values for each input variable due to the data was not available at once. With this in mind, it was demonstrated that if enough historical data are available to generate an autoregressive model, the system can converge to the optimum of the plant.

It Future work should advance the time reduction in the data collection for the stage of estimation of gradients, which is the main disadvantage of the method presented herein, where it is necessary to have as many measures in steady state as input variables to the system, that is either disturbance and decision variables. Furthermore, extracting gradient information from the historical database using other methodologies is suggested.

Acknowledgments

The researchers want to give thanks for the financial support of CONICYT-FONDECYT through its project No. 11160203, and the grant PIIC program of UTFSM.

References

Bamberger, W., and Isermann, R. (1978). Adaptive on-line steady-state optimization of slow dynamic processes. *Automatica, 14*(3), 223-230.

Bergh, L. (2007). Combining on-line process measurements and models to empirically test strategies for process monitoring, diagnosis and control. *IFAC Proceedings Volumes, 40*(11), 363-368.

Bergh, L. (2012). A Hybrid Approach to Empirically Test Process Monitoring, Diagnosis and Control Strategies *Advanced Information Technology in Education* (pp. 215-222): Springer.

Bergh, L., and Yianatos, J. (1993). Control alternatives for flotation columns. *Minerals Engineering, 6*(6), 631-642.

Bergh, L., and Yianatos, J. (2011). The long way toward multivariate predictive control of flotation processes. *Journal of process control, 21*(2), 226-234.

Bergh, L., and Yianatos, J. (2014). Engineers training in automation of flotation processes. *IFAC Proceedings Volumes, 47*(3), 11488-11493.

Bergh, L., Yianatos, J., and Leiva, C. (1998). Fuzzy supervisory control of flotation columns. *Minerals Engineering, 11*(8), 739-748.

Box, G. E. P., Jenkins, G. M., Reinsel, G. C., and Ljung, G. M. (2015). *Time Series Analysis: Forecasting and Control*: Wiley.

Brdys, M., and Tatjewski, P. (1994). An algorithm for steady-state optimizing dual control of uncertain plants. *IFAC Proceedings Volumes, 27*(11), 215-220.

Brdys, M. A., and Tatjewski, P. (2005). *Iterative Algorithms for Multilayer Optimizing Control*: Imperial College Press.

Bunin, G. A., François, G., and Bonvin, D. (2012). *Exploiting local quasiconvexity for gradient estimation in modifier-adaptation schemes*. Paper presented at the American Control Conference (ACC), 2012.

Coordinador eléctrico nacional (2017). Resumen ejecutivo de operación. 08-05-2017. Retrieved 03-11-2017 from https://sic.coordinadorelectrico.cl/wp-content/uploads/2017/05/Resumen-Ejecutivo-de-Operaci%C3%B3n-08-05-2017..pdf

Costello, S., François, G., and Bonvin, D. (2016). A directional modifier-adaptation algorithm for real-time optimization. *Journal of process control, 39*, 64-76.

Chachuat, B., Srinivasan, B., and Bonvin, D. (2009). Adaptation strategies for real-time optimization. *Computers & chemical engineering, 33*(10), 1557-1567.

Darby, M. L., Nikolaou, M., Jones, J., and Nicholson, D. (2011). RTO: An overview and assessment of current practice. *Journal of process control, 21*(6), 874-884.

Finch, J. A., and Dobby, G. S. (1990). *Column flotation*: Pergamon Press.

François, G., and Bonvin, D. (2013). Use of transient measurements for the optimization of steady-state performance via modifier adaptation. *Industrial & engineering chemistry research, 53*(13), 5148-5159.

Gao, W., and Engell, S. (2005). Iterative set-point optimization of batch chromatography. *Computers & chemical engineering, 29*(6), 1401-1409.

Gao, W., Wenzel, S., and Engell, S. (2016). A reliable modifier-adaptation strategy for real-time optimization. *Computers & chemical engineering*.

Ipinza, J. (2009). El consumo específico de energía. *Minería chilena*. Retrieved from http://www.mch.cl/reportajes/el-consumo-especifico-de-energia/

Mansour, M., and Ellis, J. (2003). Comparison of methods for estimating real process derivatives in on-line optimization. *Applied Mathematical Modelling, 27*(4), 275-291.

Marchetti, A., Chachuat, B., and Bonvin, D. (2009). Modifier-Adaptation Methodology for Real-Time Optimization. *Industrial & engineering chemistry research, 48*(13), 6022-6033.

Marchetti, A., Chachuat, B., and Bonvin, D. (2010). A dual modifier-adaptation approach for real-time optimization. *Journal of process control, 20*(9), 1027-1037.

Marchetti, A., François, G., Faulwasser, T., and Bonvin, D. (2016). Modifier Adaptation for Real-Time Optimization—Methods and Applications. *Processes*, *4*(4), 55.

Navia, D., Briceño, L., Gutiérrez, G., and De Prada, C. (2015). Modifier-Adaptation Methodology for Real-Time Optimization Reformulated as a Nested Optimization Problem. *Industrial & engineering chemistry research*, *54*(48), 12054-12071.

Navia, D., Villegas, D., Cornejo, I., and de Prada, C. (2016). Real-time optimization for a laboratory-scale flotation column. *Computers & chemical engineering*, *86*, 62-74.

Rhinehart, R. (1995). *A novel method for automated identification of steady-state*. Paper presented at the American Control Conference, Proceedings of the 1995.

Roberts, P. (1979). An algorithm for steady-state system optimization and parameter estimation. *International Journal of Systems Science*, *10*(7), 719-734.

Rodríguez-Blanco, T., Sarabia, D., Pitarch, J., and de Prada, C. (2017). Modifier Adaptation methodology based on transient and static measurements for RTO to cope with structural uncertainty. *Computers & chemical engineering*, *106*, 480-500.

Savassi, O. (2005). A compartment model for the mass transfer inside a conventional flotation cell. *International journal of mineral processing*, *77*(2), 65-79.

Tatjewski, P. (2002). Iterative optimizing set-point control–the basic principle redesigned. *IFAC Proceedings Volumes*, *35*(1), 49-54.

Wenzel, S., Gao, W., and Engell, S. (2015). Handling Disturbances in Modifier Adaptation with Quadratic Approximation** The research leading to these results was funded by the ERC Ad-vanced Investigator Grant MOBOCON under the grant agreement No. 291458. *IFAC-PapersOnLine*, *48*(25), 132-137.

Yianatos, J., Bergh, L., and Cortés, G. (1998). Froth zone modelling of an industrial flotation column. *Minerals Engineering*, *11*(5), 423-435.

Yianatos, J., Bucarey, R., Larenas, J., Henríquez, F., and Torres, L. (2005). Collection zone kinetic model for industrial flotation columns. *Minerals Engineering*, *18*(15), 1373-1377.

Yianatos, J., Finch, J., and Laplante, A. (1986). Holdup profile and bubble size distribution of flotation column froths. *Canadian Metallurgical Quarterly*, *25*(1), 23-29.